One-dimensional excitons in GaAs quantum wires

1998 J. Phys.: Condens. Matter 10 3095

(http://iopscience.iop.org/0953-8984/10/14/004)

J. Phys.: Condens. Matter **10** (1998) 3095–3139. Printed in the UK PII: S0953-8984(98)82817-8

REVIEW ARTICLE

One-dimensional excitons in GaAs quantum wires

Hidefumi Akiyama

Institute for Solid State Physics (ISSP), University of Tokyo, 7-22-1 Roppongi, Minato-ku, Tokyo 106, Japan

Received 15 December 1997

Abstract. The elementary properties of one-dimensional (1D) excitons in GaAs quantum wires (QWRs) in the strong-confinement regime have been reviewed in order to investigate the novel physics inherent to 1D systems. We first overview the energy levels realized in various QWRs such as T-shaped, V-groove, vicinal-substrate, and post-growth-etching QWRs. Then we study lateral confinement energy, exciton binding energy, the Bloch part and the envelope part of the wave functions, oscillator strength, lifetime, laser action, and other properties such as many-body effects and relaxation processes. A set of experimental data are given as examples, mostly taken from the recent work on T-shaped QWRs by the author and co-workers, and there is some discussion of these data.

1. Introduction

Thanks to recent advances in the fabrication technology for producing nanometre-sized semiconductor quantum structures [1, 2], a substantial number of experiments have already been performed on the optical properties of quantum wires (QWRs). The purpose of this article is to review those experiments and to discuss the novel physics of electron–hole pairs, or excitons, formed in one-dimensional (1D) systems. A series of experimental data are presented as examples, mostly taken from the recent work by Sakaki, Someya, Akiyama (SSA), and their co-workers, and there is some discussion of these data.

Although various types of QWR have already been realized using III–V, II–VI, and Si_xGe_{1-x} semiconductor heterostructures, and also using porous Si, polymers, and colloids, we restrict this study to GaAs-related QWRs formed by means of such epitaxial growth techniques as molecular-beam epitaxy (MBE) and metallo-organic chemical vapour deposition (MOCVD), for the following reasons.

Among the various heterostructures and low-dimensional structures, GaAs-related heterostructures are unique in that their electronic states and optical properties can be described in the effective-mass approximation almost purely quantum mechanically, free from the complexity of the materials, with the constituent materials represented by a few band parameters. In addition, no interface states are formed at hetero-interfaces in the well-established epitaxial growth mode. The lattice is rigid, so the lattice distortion due to the optical transition from the valence band to the conduction band is negligible. In fact, the physics of 2D excitons in GaAs QWs—such as the room temperature excitonic absorption, the quantum-confined Stark effect, and resonant tunnelling—are well understood quantum mechanically [3]. We aim to discuss the novel physics of 1D excitons along these lines.

As regards the size of the QWRs, we limit our discussion to small QWRs with cross-sectional sizes at least below the Bohr diameter of 3D excitons in bulk, which is about 20 nm

0953-8984/98/143095+45$19.50

for GaAs. Such confinement is called strong confinement, or individual confinement, and in this type of confinement the quantization energy of individual electrons and holes dominates over the energy of the Coulomb interaction between them. Excitons are formed from 1D electrons and 1D holes confined individually; these are called 1D excitons in the rigorous sense. In the case where the cross-sectional size of the wire structure is larger than the Bohr diameter of 3D excitons, only the centre-of-mass motion of the 3D excitons is quantized. Such confinement is called centre-of-mass confinement, or weak confinement.

To realize strong confinement in GaAs, the QWR size should be around 10 nm or less. This is a requirement that is hard to meet, since atomic order fluctuation of the interface causes a substantial broadening in that region. The broadening must be smaller than the energy of interest for the 1D excitons, while the confinement energy must be significantly larger than it. In the approximation of an infinitely high barrier, the broadening is proportional to the inverse of the cube of the size—that is, to the 3/2 power of the quantization energy. Not only is the smallness of the size important, but so also is the smallness of the size fluctuation. Atomic order uniformity in QWRs is necessary for our purpose. Because of this requirement, the samples of QWR useful for the study of the physics of 1D excitons are very limited.

For QWs, thickness is the only structural parameter, except the band parameters of the constituent materials. For QWRs, however, the structure is defined by the 2D cross-sectional shape. The cross-sectional shape of the resultant QWRs varies according to the fabrication method, which leads to varied confinement geometry. In fact, our main concern is to understand how the properties of 1D excitons in QWRs vary accordingly to the confinement.

We start this review by investigating the energy levels realized in QWRs in relation to the various confinement geometries in section 2. Although the detailed discussion of the resultant energy levels includes the interesting physics of lateral confinement energy and exciton binding energy inherent to 1D systems, we examine these points separately in sections 3 and 4. Next, we investigate the Bloch parts of the wave functions in QWRs in section 5 and the envelope parts of the wave functions in QWRs in section 6; these are studied via optical anisotropy and magneto-photoluminescence measurements, respectively. Then, in sections 7–9, we deal with the optical transition properties of 1D excitons, namely the oscillator strength, the exciton lifetime, and the laser action. In section 10, we discuss the remaining properties, such as many-body effects, and relaxation processes of 1D excitons, and some particular properties and measurements of interest. The final section is devoted to some notes added to conclude this review.

2. Characterization of energy levels

The characterization of the energy levels is firstly important in the understanding of the confinement geometry in the respective QWRs. For this purpose, photoluminescence (PL) spectroscopy is useful, since it is easy to carry out and has high sensitivity. To characterize higher energy levels, PL excitation (PLE) spectrum measurements are used. Advanced subjects like the exciton binding energy, based on the characterization of the energy levels, are discussed separately in sections 3 and 4.

Since the current fabrication of QWRs is mostly based on a modified hetero-epitaxial thin-film growth technique, QWRs are formed using the edges, corners, or intersections of 2D QW layers. Therefore, the confinement in the QWRs is achieved in two steps, where the first strong confinement into the QW layers (perpendicular confinement) is achieved by means of the potential barriers of the heterostructures, and the second weaker confinement into the QWRs within the layers (lateral confinement) is realized as a result of the difference

of the quantization energy from that of the stronger confinement.

The main aim of the energy level characterization is to evaluate the lateral confinement and the stability of the 1D excitons achieved, on the basis of quantized energy levels in QWRs. An additional aim is the evaluation of the broadening and Stokes shift, which represent the uniformity of the structures and the effect of localization. The confinement geometry and uniformity depend very much on which method is used to fabricate the QWR; the methods are briefly described at the beginning of each subsection below. For the details of the fabrication methods and their structural characteristics, readers should consult other articles [1, 2]. Efforts to improve the fabrication methods are important for extending the studies of the 1D physics of QWRs; some of them will be emphasized in this review.

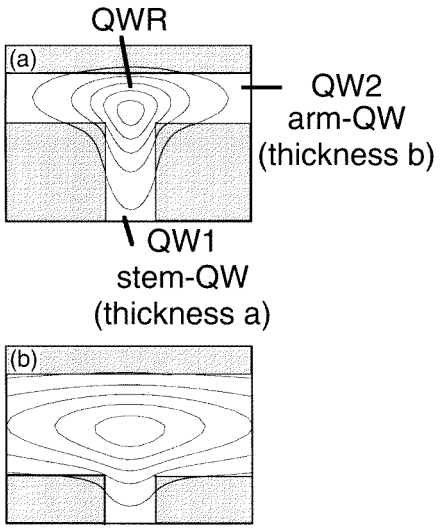

Figure 1. The T-shaped QWR is formed at the T intersection of the first QW (QW1 or the stem-QW, with thickness a) and the second QW (QW2 or the arm-QW, with thickness b). The contours of constant probability ($|\psi|^2 = 0.1$, 0.3, 0.5, 0.7, and 0.9) for electrons confined at the QWR states are calculated for GaAs/$Al_{0.3}Ga_{0.7}$As T-QWRs with (a) $a = b = 5$ nm and (b) $a = 5$ nm, $b = 10$ nm. (Reproduced from reference [17].)

2.1. T-shaped and related quantum wires

The concept of the T-shaped QWR (T-QWR) structure was originally proposed by Chang, Chang, and Esaki [4] in 1985. As schematically shown in figure 1, the 1D electronic state is formed at the T intersection of two parent QWs, namely the first QW (QW1) forming the 'stem' part of the letter 'T' and the second QW (QW2) forming the 'arm' part of it. In 1990, the cleaved-edge-overgrowth (CEO) method, with MBE, was developed by Pfeiffer and co-workers at Bell Laboratories, which enabled us to combine two thin-film growth processes in two different directions to define QWRs [5–7], as schematically shown in figure 2. In fact, they fabricated the T-QWR structure by the CEO method, showed PL [8] in 1992, and demonstrated laser action by means of optical pumping [9] in 1993 and by means of current injection [10] in 1994. The physics of 1D excitons has been intensively studied in the T-QWR structure. Although its history is short, the T-QWR structure has up to now proved one of the most useful QWR structures for 1D exciton study, and it is

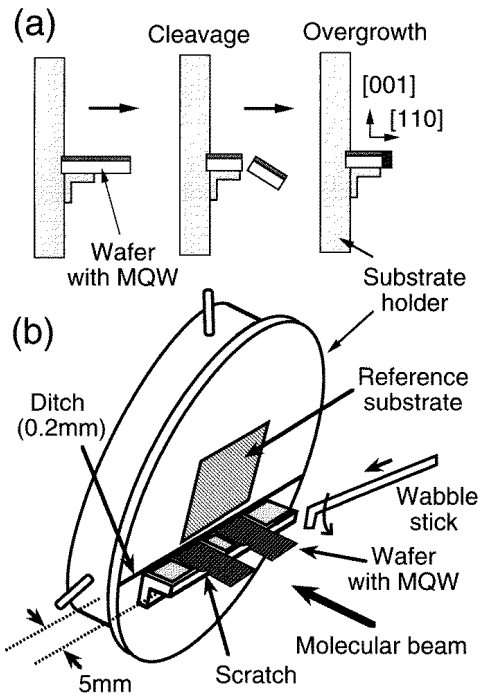

Figure 2. (a) The principle of the cleaved-edge-overgrowth (CEO) method developed originally by Pfeiffer *et al*. The MQW is grown firstly by the conventional MBE growth method. After thinning and mounting the wafer with the MQW vertically on the special substrate holder, *in situ* cleavage of the wafer is carried out. Then heterostructures are overgrown on the (110) cleaved surface. (b) A schematic illustration of the substrate holder for the CEO method. Two pieces of 90 μm-thick wafer with MQWs are mounted vertically on the substrate holder. The pieces are cleaved one after another by a wabble stick, and then overgrown within a few seconds of the cleavage. (Reproduced from reference [7].)

the structure that we most frequently discuss in this review [7–24].

In general, the study of QWRs requires the characterization of cross-sectional structures (size and shape). For this purpose, a transmission electron microscope (TEM), a scanning electron microscope (SEM), a scanning tunnelling microscope (STM), or an atomic force microscope (AFM) is usually needed. However, concerning T-QWRs made by the CEO method with high controllability, the size and shape are given by the energy levels of the parent QWs, namely QW1 and QW2. With the adoption of elaborate design of the whole sample structure, the energy levels were precisely determined simply by means of conventional microscopic PL measurements.

Figure 3 shows the schematic structure of a 5 nm-scale GaAs/AlAs T-QWR sample and its spatially resolved PL spectra, from a paper by SSA [14].

The sample was fabricated [7] in the following way. In the first growth, SSA prepared a multi-QW structure, which consists of $n = 50$ periods of GaAs QWs (QW1, thickness $a = 5.3$ nm) separated by AlAs barriers (thickness $c = 50$ nm) in between. After the cleavage, they overgrew on the (110) cleaved surface a GaAs QW layer (QW2, thickness $b = 4.8$ nm), an 8 nm-thick AlAs barrier layer, a reference QW layer for QW2 (QW2-u, thickness $b = 4.8$ nm), a 20 nm-thick AlAs barrier layer, and then a 30 nm-thick GaAs cap layer. The overgrowth was carried out at the substrate temperature of 500 $^\circ$C at the

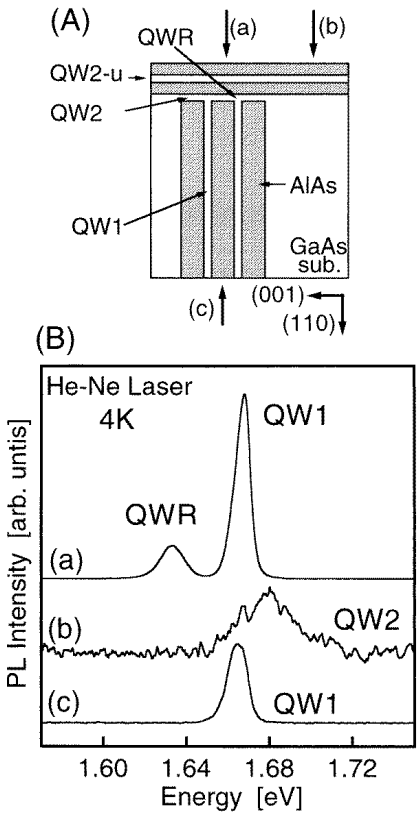

Figure 3. (A) The structure of a T-shaped quantum wire sample together with the geometry of the experiment. The arrows (a), (b), and (c) indicate the direction of the incident light when the photoluminescence spectra (a), (b), and (c) in (B) were measured, respectively. (B) PL spectra were measured at 4 K for three different excitation geometries. The excitation was by a He–Ne laser beam with diameter of 2 μm. Curves (a) and (b) were obtained when the excitation beam was moved along the (110) overgrown layer from the region of wire arrays to the substrate. Spectrum (c) was measured when the excitation laser beam was incident on the (110) surface of a multi-quantum-well (QW1) wafer without overgrowth. (Reproduced from reference [14].)

growth rate of 0.3 μm h^{-1} for GaAs and the V/III flux ratio of 30. As shown in figure 3, QWRs were formed at the intersection of the multi-QW layer (QW1) and the overgrown QW (QW2).

In general, to realize strong lateral confinement in T-QWRs, the thickness a of QW1 and the thickness b of QW2 must be sufficiently small ($<$10 nm), and they must be set close to each other. To prevent the quantum coupling of QWRs, the interwire interval c, or the barrier thickness of QW1, must be sufficiently thick and typically larger than 30 nm. Otherwise, the continuum states corresponding to QW2 and QWR states tend to merge or mix, which modifies the quantized energy of the QW2 and QWR states.

The QW2-u layer that has the same thickness as QW2 was introduced to facilitate the measurement of the QW2 energy level. Although the PL lines from QWR and QW1 are usually observed for T-QWR structures formed by the CEO method, the PL from QW2 is difficult to measure since most carriers diffuse from the region of QW2 to that of the QWR. This problem can be avoided in QW2-u since there is no carrier diffusion from QW2-u to the

QWR region. Because QW2-u was grown after the growth of QW2, the thicknesses of the two GaAs layers were identical within an accuracy of one-monolayer (1 ML = 0.283 nm) fluctuation. Hence QW2-u should have the same energy as QW2, so we can determine the energy level of QW2.

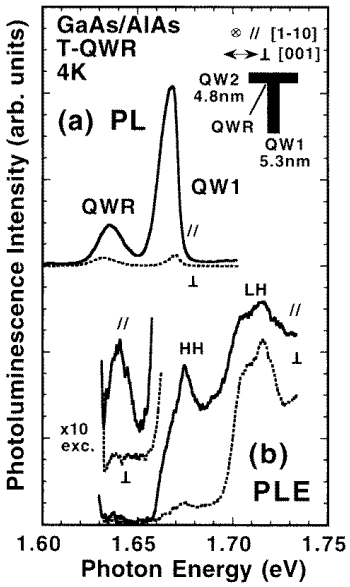

Figure 4. PL (a) and PLE (b) spectra measured at 4 K for the 5 nm-scale GaAs/AlAs T-QWR sample. The polarization of the light for detection in PL and excitation in PLE was parallel (∥, solid curves) or perpendicular (⊥, broken curves) to the QWRs. The excitation laser energy was 1.72 eV in the PL measurements. The detection energy in the PLE measurements was 1.625 eV, which is in the low-energy tail of the QWR. The magnified PLE spectra were measured with ten-times-higher excitation intensity. (Reproduced from reference [19].)

The PL spectra were measured at 4 K using a He–Ne laser. The PL spectra are obtained from the (110) surface in the backward-scattering geometry. Two PL peaks were clearly observed in curve (a), and were assigned as indicated in figure 3. The higher-energy peak was attributed to QW1, and the lower-energy peak was identified as originating from the QWR.

This identification was made by performing a spatially resolved PL measurement. Curve (a) of figure 3 was obtained when the excitation laser beam (with the diameter of 2 μm) was incident primarily onto the region containing QWRs. Curve (b) was obtained when the excitation laser beam was moved along the overgrown plane towards the substrate. Curve (c) was obtained when the beam was incident on the (110) surface of the multi-QW wafer (QW1) without overgrowth. It is now clear that the PL peak in curve (b) originates from QW2-u whereas the PL peak in curve (c) arises from QW1. The PL peak that has the lowest energy appears only in curve (a), which indicates that this PL peak arises from QWRs. One should note that the intensity of the QWR PL is stronger than that of the QW2-u PL although the volume of the QWRs is quite small. This is due to the efficient diffusion of carriers from the regions of QW1 and QW2 into the QWR region, which has a lower energy.

The energies of the PL peaks arising from QW1, QW2, and the QWR are all directly

shown in the spectra. The important quantity here is E^*_{1D-2D} defined as the energy difference between the 1D exciton in the QWRs and the lowest 2D exciton in either QW1 or QW2. We call E^*_{1D-2D} the effective lateral confinement energy of excitons in QWRs. We denote the energy difference between individual electrons (holes) in the QWRs and those in the parent QWs as E_{1D-2D}, the lateral confinement energy of electrons (holes).

Since QW2 is a little thinner than QW1, the PL from QW2 has a slightly higher energy than that from QW1. Hence, E^*_{1D-2D} for the T-QWR is equal to the energy spacing between the QWR peak and the QW1 peak, and is found to be 35 meV for our sample. Note that the value of E^*_{1D-2D} is 35 meV, which is above the thermal energy $k_BT = 26$ meV at 300 K. This result indicates that most electrons and holes can be accommodated in the ground states of T-QWRs even at room temperature. Further systematic study of E^*_{1D-2D} is described in the next section.

Figure 4 shows the PL and PL excitation (PLE) spectra of a 5 nm-scale GaAs/AlAs T-QWR sample measured with a Ti:sapphire laser [19]. The solid and dashed curves show the data for the polarization parallel and perpendicular to the QWRs, respectively. The polarization dependence is discussed later in a separate section. Note that in the PLE spectra the small 1D exciton peak for the QWRs is the only peak on the lower-energy side of the 2D exciton peak for QW1. This manifests the theoretically known fact that such T-QWRs, made of only two kinds of material, for the barrier and the well, are single-mode QWRs which have only one 1D electron subband in the structures.

The Stokes shift is an important quantity to evaluate from the PL and PLE measurements. The values of the PL linewidth and the Stokes shift are 15 meV and 5 meV for QWRs, respectively, and 10 meV and 7 meV for QW1. These demonstrate the high quality of the sample, and the free-excitonic nature of the origins of the respective PL peaks.

There have been other interesting directions taken in efforts to realize large values of E^*_{1D-2D}. Pfeiffer and co-workers [13] proposed and studied double-stem T-QWRs, which are Π-geometry QWRs, using a stem consisting of two QWs separated by a thin but opaque barrier. They have shown that the value $E_{1D-2D} = 28$ meV achieved for electrons in 3 nm-scale T-QWR structures with 500 meV barrier energies can be increased by 5.5 meV by the double-stem technique. In this case, the QWR is not a single-mode QWR.

The next type of modification is asymmetric T-QWRs formed with QW1 and QW2 composed of different materials, such as $Al_xGa_{1-x}As$ for QW1 and GaAs for QW2. In fact, this was the original T-QWR structure proposed by Chang, Chang, and Esaki [4], and it was first experimentally studied by Goñi and co-workers [8]. By combining a rather thick $Al_xGa_{1-x}As$ QW1 and a thinner GaAs QW2, Hasen and co-workers [25] achieved $E^*_{1D-2D} = 40$ meV. Gislason, Langbein, and Hvam [26, 27] studied T-QWRs each consisting of a 12 nm-thick $Al_{0.14}Ga_{0.86}As/Al_{0.3}Ga_{0.7}As$ QW1 and a 3 nm-thick $GaAs/Al_{0.3}Ga_{0.7}As$ QW2 to demonstrate that $E^*_{1D-2D} = 54$ meV can be obtained.

Another type of QWR fabricated by a similar CEO method, but based on a different confinement mechanism, are the strain-induced QWRs studied by Gershoni and co-workers [28–30].

They first grew 150 periods of strained-layer superlattice (SL) of 7.1 nm-thick $In_{0.063}Ga_{0.937}As$ and 24 nm-thick GaAs. On the cleaved edge of the strained-layer SL, they grew 8 nm-thick and 3.4 nm-thick $GaAs/Al_{0.3}Ga_{0.7}As$ QWs. The QWs were separated from the cleaved edge and from each other by 20 nm-thick $Al_{0.3}Ga_{0.7}As$ barrier layers. Since the lattice constant of $In_{0.063}Ga_{0.937}As$ is larger than that of GaAs, the region overgrown on $In_{0.063}Ga_{0.937}As$ by the CEO method should have expanding strain resulting in decreased band-gap energy compared with that of the region overgrown on GaAs. They reported $E^*_{1D-2D} = 20$ meV for the lowest exciton transition.

2.2. V-groove and related quantum wires

Kapon and co-workers [31, 32] developed and reported in 1987 a novel selective-growth method using MBE on non-planar substrates to achieve lateral confinement by QW thickness variation. In 1989, they realized crescent-shaped QWRs by a MOCVD selective-growth method on V grooves defined by conventional photolithography and wet chemical etching, and demonstrated laser action by current injection [33]. Since then, this type of QWR (V-groove QWRs) have been studied and developed all over the world. Although the lateral size of the active region in the first QWR laser structure was as large as several tens of nanometres, continuous effort has reduced it to around 10 nm. With holographic photolithography to define V grooves, high-density arrays of such QWRs are available. The V-groove QWR structure is now one of the most familiar QWR structures, with a large number of publications devoted to them. They are discussed selectively from the viewpoint of 1D physics in this review [33–52].

Gustafsson and co-workers recently reported [41] improved V-groove QWR structures grown by low-pressure MOCVD on a (100) GaAs substrate patterned with a grating of V grooves made along $[01\bar{1}]$ by wet chemical etching. The growth on the V groove exhibits a self-limiting growth profile, so the curvatures ρ_{sl} of the bottom interfaces are controlled by the atom migration length inherent to the material and the growth conditions. In fact, the curvatures of $Al_xGa_{1-x}As$ surfaces and GaAs surfaces were reproduced in the vertical stack of three repeated crescents. Because of the segregation of the group III species, Ga-rich vertical QW (VQW) structures were formed in the $Al_xGa_{1-x}As$ alloy in the V groove. The layer thickness in the bottom crescents is far larger than that of the neighbouring QWs, so crescent QWRs are formed.

Gustafsson and co-workers measured cathodoluminescence (CL) spectra [41] at various excitation densities of a single-GaAs-QWR crescent structure similarly fabricated to have 8 nm thickness at the crescent corner and $\rho_{sl} = 4.9 \pm 0.2$ nm radius of curvature. In the CL spectra obtained under low excitation density, three CL peaks arising from the QWR, QW and VQW were observed at 1.57 eV, 1.74 eV, and 1.89 eV, respectively. The CL width of the QWRs was about 20 meV.

As the excitation density is increased, CL from the higher subbands ($n = 2$ and 3) in QWRs is observed as additional peaks at 1.605 eV and 1.64 eV, respectively. The subband energy separation $E^*_{12,\mathrm{QWR}}$ of the $n = 1$ optical transition and $n = 2$ transition in the QWRs was 35 meV. In multimode QWRs having multiple subbands, the subband energy separation $E^*_{12,\mathrm{QWR}}$ is an important quantity for characterizing the lateral confinement. Note that the value of $E^*_{12,\mathrm{QWR}}$ is above the thermal energy $k_BT = 26$ meV at 300 K, indicating the stability of electrons and holes in the ground states of QWRs.

Clear PLE spectra were recently reported [42] for two samples of QWR crescent structures. The samples were fabricated, similarly to the previous samples, with nominal GaAs thicknesses of 1.5 nm (a) and 2.5 nm (b), and in practice had 4.1 and 8.8 nm thicknesses at the crescent centres, respectively. The width of the PLE peak and the Stokes shift were 12 meV and 8 meV for (a), while they were 8 meV and 6 meV for (b). These values as well as the clear PLE spectra indicate the high degree of uniformity of the structures. The subband energy separations $E^*_{12,\mathrm{QWR}}$ of the $n = 1$ optical transition and $n = 2$ transition in the QWRs read from the spectra were 25 meV (a) and 27 meV (b).

There are many variations in the QWR formation with selective growth on non-planar substrates using MBE and MOCVD. Sogawa and co-workers [52] formed narrow trench structures, or U grooves, with selective MOCVD growth on the V grooves, in which they fabricated buried QWRs with rectangular cross-sectional shapes of 20 nm width.

They fabricated four GaAs/AlAs rectangular QWR samples with sizes of 20 nm × 16 nm, 20 nm × 11 nm, 20 nm × 11 nm, and 17 nm × 10 nm. Their PL and PLE spectra were well reproduced by theoretical calculation for the rectangular QWRs. Although the lateral size is as large as 17–20 nm, the QWRs are surrounded by AlAs barriers both vertically and laterally, resulting in complete 2D confinement. In fact, the subband energy separation $E^*_{12,\mathrm{QWR}}$ of the $n = 1$ and $n = 2$ optical transitions in the QWRs read from the PLE spectra was large, 35–54 meV.

Crescent QWRs are formed not only in the bottoms of grooves, but also on the ridge top via the selective-growth methods. Koshiba and co-workers [53–56] formed ridge structures via MBE facet growth on inverse-mesa patterned substrates. The QWR structures are formed as curved QW layers formed on top of the sharp ridges. The curvature of the ridge structure was controlled by the growth conditions.

2.3. Vicinal-substrate quantum wires

Among the various methods of fabrication of QWRs proposed and developed so far, the step flow mode of growth on vicinal substrates with MBE or MOCVD is one of the most intensively studied techniques. Vicinal surfaces with small misorientation angles have an atomic step array with a well-defined periodicity in the 10 nm range. In the step flow growth mode, preferential adsorption of growing species impinging on the terraces occurs at the step edges. Petroff and co-workers [57–59] investigated, in this mode, the repeated deposition of partial layers of different compositions, and then applied it to the formation of a lateral superlattice (SL) whose composition is modulated with the periodicity of the atomic steps in the vicinal substrates. On the basis of this technique, lateral confinement was demonstrated in tilted- (lateral or fractional) SL QWRs [58, 60, 61], grid-inserted QWRs [62], and serpentine-SL QWRs [63, 64].

One of the major problems, in making GaAs/AlAs tilted-SL QWRs for example, lies in the imperfect step flow growth of Al [59]. The Al atoms are thermodynamically and kinetically difficult to incorporate just at the step edge and not out on the terrace. Furthermore, the exchange of Al atoms with the previously deposited Ga atoms occurs on the terrace. As a result, the Al composition of the wells and barriers in the tilted SL is averaged, which weakens the composition modulation. In fact, experiments have been consistent in yielding the interpretation that the conduction electron states are rather strongly coupled and hence 2D-like in such QWRs, while the hole states are laterally confined into 1D-like states.

It should be commented that, although the achievement of strong lateral confinement is still difficult, such unique periodic lateral modulation of exciton states in QWs has been applied in some advanced studies of exciton physics, which are cited in later sections [61–70].

In addition, coherent multi-atomic steps with straight edges formed on vicinal or high-index-oriented substrates have been found and studied with a view to the formation of QWRs in the strong-lateral-confinement regime [71–73].

2.4. Etched quantum wires

The most direct way to fabricate QWRs is post-growth etching of structures with QWs. That is, QWs are first grown by the conventional MBE or MOCVD method, and these are then processed into QWR structures by photolithography, electron-beam lithography, or holographic lithography, and dry or wet etching [1].

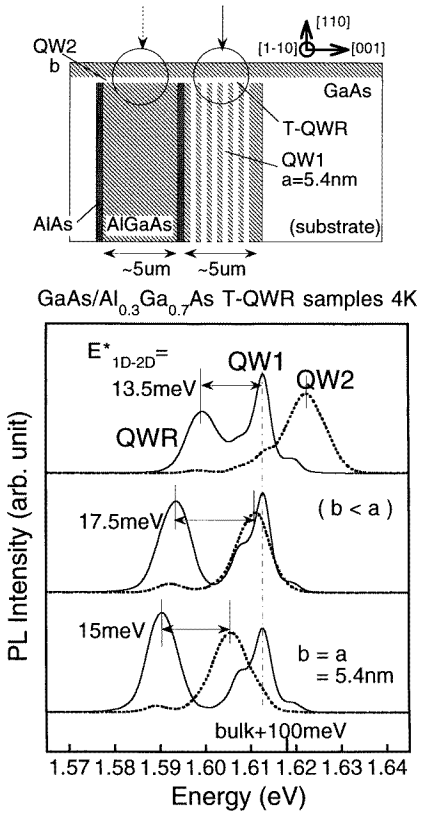

Figure 5. A schematic diagram of the structure of 5 nm-scale $GaAs/Al_{0.3}Ga_{0.7}As$ T-QWR samples and the spatially resolved PL spectra at 4 K for three T-QWR samples with identical QW1 thickness a and different QW2 thicknesses b. Solid (broken) curves show the PL for the region with T-QWRs (a 5 μm-wide QW2) indicated by a solid (broken) arrow in the sample structure. The effective lateral confinement energy of excitons, E^*_{1D-2D}, is defined as the difference in energy between the 1D exciton in a T-QWR and the lowest 2D exciton in either QW1 or QW2. (Reproduced from references [16, 22].)

One of the problems was degradation of the PL for narrow QWRs due to the damaged or optically inactive region formed at the etched side-wall surface [74, 75], although overgrowth to cover the QWRs [76] and passivation [77] have been attempted to reduce the damage.

To prevent such serious damage, a method for etching just the top (covering) layers of the QWs was developed. Although the mechanism of lateral confinement there is not fully understood, it is thought that the lateral confinement is introduced via strain and electrostatic fields [78, 79]. In 1989, Kash and co-workers [80] extended this method by using strained layers to cover QWs, and realized strain-induced QWRs with patterned stressors on top.

Another problem with these QWRs has been the difficulty of producing width narrowing and/or deep energy modulation to achieve the strong lateral confinement instead of the weak centre-of-mass lateral confinement. There are similar problems for QWRs formed by ion-implantation-induced intermixing of QWs [81]. Although various seminal spectroscopic studies of excitons have been made for these QWRs [82–94], the observed phenomena are for excitons in the weak-lateral-confinement regime, and are not within the main scope of this paper.

3. Lateral confinement energy

As discussed briefly in the previous section, it is essential in QWR study to evaluate the energy scale which characterizes the lateral confinement. In single-mode QWRs with only one 1D subband, the lateral confinement of electrons or holes is characterized by the energy difference E_{1D-2D} between the lowest 1D and 2D electronic states. In multimode QWRs with multiple 1D subbands, it is characterized by the first and second subband spacing $E_{12,QWR}$ in the QWRs. These quantities show not only the strength of the lateral confinement, but also the stability of the ground 1D state. For excitons, or optical transitions between the hole and electron states, we denote these values as E^*_{1D-2D} and $E^*_{12,QWR}$, including the Coulomb interaction energy, which are called the effective lateral confinement energies of excitons.

A systematic study of the effective lateral confinement energy of excitons has been carried out on several series of T-QWRs by SSA [7, 16, 20, 22, 23], and this is the main subject of this section. The T-QWRs made of only two kinds of material, for the barrier and the well, are single-mode QWRs which have only one 1D electron subband in the structures, so E^*_{1D-2D} is the effective lateral confinement energy of excitons in T-QWRs. On the basis of the systematic study of E^*_{1D-2D} made for T-QWRs, the stability and dimensionality of 1D excitons have been examined.

In this section, we also describe the design of the particular sample structures, using which all of the PL lines from the QWRs, QW1, and QW2 can be detected and identified uniquely by the spatially resolved PL technique, in order to determine E^*_{1D-2D}. We should note that, for any T-QWR samples fabricated successfully, PL spectra for the QWR and QW1 are easily detected, while the PL from QW2 is not always observed because of the fast-carrier diffusion from the QW2 region to the QWR region [9, 15]. This feature is analogous to the familiar fact that PL spectra from multi-QW structures are usually dominated by the QWs rather than the barriers, since carriers generated in the barrier region are efficiently collected by the QW region.

3.1. 5 nm-scale GaAs/$Al_{0.3}Ga_{0.7}$As T-QWRs

Figure 5 shows schematically the structure of 5 nm-scale GaAs/$Al_{0.3}Ga_{0.7}$As T-QWR samples and their spatially resolved PL spectra at 4 K; it is reproduced from the work by SSA [16, 22].

The samples were fabricated as follows. The multiple-QW structure (QW1) consists of $n = 50$ periods of GaAs QWs (of thickness $a = 5.4$ nm) and $Al_{0.3}Ga_{0.7}As$ barriers (of thickness $c = 100$ nm), and is about 5 μm thick in total. An additional 5 μm-thick $Al_{0.3}Ga_{0.7}As$ layer is formed in the first growth, which results in a 5 μm-wide area of QW2 after CEO. The overgrown QW (QW2) is composed of a GaAs layer (of thickness b), covered with an $Al_{0.3}Ga_{0.7}As$ barrier layer. SSA performed several CEO runs with different QW2 thicknesses b and constant QW1 thickness, prepared by cutting one substrate wafer into many pieces after the first MBE growth was complete. In this way, they obtained a series of samples, for which a was constant, while the thickness b of QW2 was varied around a.

The spatially resolved PL spectra shown in figure 5 are for three T-QWR samples with identical QW1 thickness a and different QW2 thicknesses b at 4 K. The PL was detected via the (110) surface in the backward-scattering geometry for normal incidence [19]. Solid (broken) curves show the PL for the region with T-QWRs (a 5 μm-wide QW2) indicated by a solid (broken) arrow in the sample structure. The PL spectra of each sample have three

peaks assigned to the heavy-hole (HH) excitons in the T-QWR, QW2, and QW1, as shown in the figure. The observed PL linewidths are only 5–8 meV, showing the high quality of the hetero-interfaces of the fabricated structures. Since the QW1 thickness a is constant, the PL peaks for QW1 appear at the same energy. On the other hand, the QW2 thickness b is varied, so the PL peaks of QW2 and the QWR are shifted. As a result, the energy levels of the T-QWRs are obtained as well as those of QW1 and QW2 for various values of b.

The bottom curves in figure 5 show the data for $a = b$, in which the PL energy level of QW2 is lower than that of QW1. This is caused by the anisotropic hole mass of GaAs. The HH mass along [001] for QW1 is $0.38m_0$, while that along [110] for QW2 is $0.71m_0$. The larger mass leads to the lower PL energy.

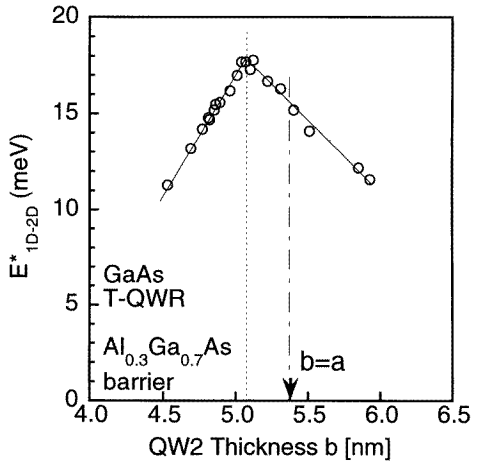

Figure 6. The effective lateral confinement energy of excitons E^*_{1D-2D} in 5 nm-scale GaAs/$Al_{0.3}Ga_{0.7}As$ T-QWR samples plotted as a function of the QW2 thickness b. Solid lines are drawn to guide the eyes. (Reproduced from reference [22].)

The effective lateral confinement energy E^*_{1D-2D} of excitons in T-QWRs is evaluated from the difference between the PL energy of a 1D exciton in a T-QWR and that of the lowest 2D exciton in either QW1 or QW2. The values of E^*_{1D-2D} for the three samples in figure 5 are found to be 13.5, 17.5, and 15 meV. These values are plotted together with data for other samples with various values of b in figure 6.

Note that E^*_{1D-2D} reaches a maximum value of 18 meV at $b = 5.1$ nm, where the energy levels of QW1 and QW2 are the same, indicating that a well-stabilized 1D state is realized. Then, E^*_{1D-2D} decreases and approaches zero as the thickness b is decreased or increased away from 5.1 nm. The decrease in E^*_{1D-2D} demonstrates how the T-QWR states deviate from the well-stabilized 1D state and take on a 2D character. Thus, E^*_{1D-2D} represents the stability and 1D nature of the excitons confined in the QWRs.

3.2. 5 nm-scale GaAs/AlAs T-QWRs

In T-QWRs, it is essential to realize a large value of E^*_{1D-2D}, the effective lateral confinement energy of excitons, in order to enhance the 1D nature of the excitons.

The straightforward way to enhance the effective lateral confinement energy E^*_{1D-2D} for T-QWRs is to enhance the quantization energy E_Q of the parent QWs (QW1 and QW2). In the infinite-barrier approximation, these two quantities should be proportional.

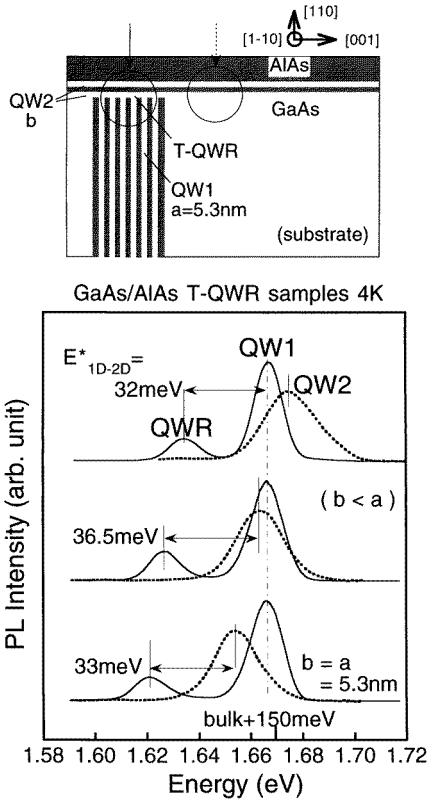

Figure 7. A schematic diagram of the structure of 5 nm-scale GaAs/AlAs T-QWR samples and the spatially resolved PL spectra at 4 K for three T-QWR samples with identical QW1 thickness a and different QW2 thicknesses b. Solid (broken) curves show the PL for the region with T-QWRs (QW2) indicated by a solid (broken) arrow in the sample structure. The effective lateral confinement energy of excitons E^*_{1D-2D} is defined as the difference in energy between the 1D exciton in a T-QWR and the lowest 2D exciton in either QW1 or QW2. (Reproduced from references [16, 22].)

In this context, SSA have increased the barrier energy by replacing the $Al_{0.3}Ga_{0.7}As$ barrier with an AlAs barrier, and performed a similar experiment on 5 nm-scale GaAs/AlAs T-QWR samples [14, 16, 19, 22]. Figure 7 shows schematically the structure of the samples and their spatially resolved PL spectra at 4 K.

The sample fabrication procedure was basically the same as that for the previous samples. Again setting a constant, SSA prepared a series of 5 nm-scale GaAs/AlAs T-QWR samples, with b gradually varied around $a = 5.3$ nm. All of the barrier layers are made of AlAs, and the structural parameters are $a = 5.3$ nm, $c = 50$ nm, and $n = 50$.

The spatially resolved PL spectra shown in figure 7 are for three T-QWR samples with identical QW1 thickness a and different QW2 thicknesses b at 4 K. The PL was detected via the (110) surface in the backward-scattering geometry for normal incidence [19]. Solid (broken) curves show the PL for the region with QWRs (the upper part of QW2) indicated by a solid (broken) arrow in the sample structure. The PL spectrum of each sample has three peaks assigned to the HH excitons in the T-QWR, QW2, and QW1, as shown in the figure. The PL linewidths of the QWRs in these samples were about 15 meV. This value is

comparable with the PL splitting of QW1 due to the fluctuation of the thickness by 1 ML, shown in figure 7, and thus is regarded as a fairly small value, showing the high quality of the hetero-interfaces of the T-QWR structures. Since the QW1 thickness a is constant, the PL peaks of QW1 appear at the same energy. On the other hand, the QW2 thickness b is varied, so the PL peaks of QW2 and the QWR are shifted.

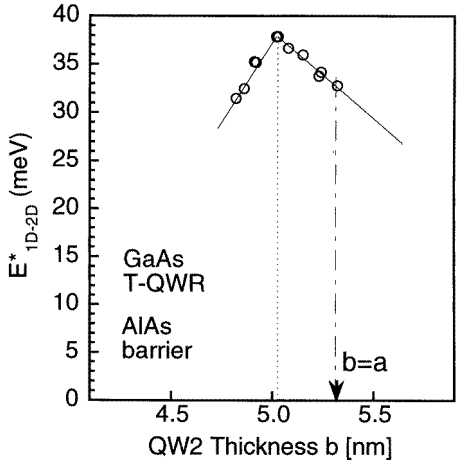

Figure 8. The effective lateral confinement energy of excitons E^*_{1D-2D} in 5 nm-scale GaAs/AlAs T-QWR samples plotted as a function of the QW2 thickness b. Solid lines are drawn to guide the eyes. (Reproduced from reference [22].)

The effective lateral confinement energy E^*_{1D-2D} of excitons in T-QWRs is evaluated from the difference in PL energy between the 1D exciton in a T-QWR and the lowest 2D exciton in either QW1 or QW2. The values of E^*_{1D-2D} of the three samples in figure 7 are found to be 32, 36.5, and 33 meV. These values are plotted together with data for other samples with various values of b in figure 8.

Due to the high AlAs barrier energy, tight confinement was realized, so increases in the quantization energy and E^*_{1D-2D} were observed. The large value of E^*_{1D-2D} beyond 30 meV supports the stable 1D electronic state, indicating potential application in room temperature devices. The maximum value of 38 meV is realized when the energy levels of QW1 and QW2 are the same.

Finally, SSA [16] plotted (see figure 9) all of the PL peak energies for 5 nm-scale GaAs/$Al_{0.3}Ga_{0.7}$As T-QWR samples and 5 nm-scale GaAs/AlAs T-QWR samples, which are the energies of the T-QWR (•), QW1 (◇), and QW2 (○) against the thickness of QW2, b. The precise dependence of the energy levels of the T-QWRs on the thickness of QW2, b, is obtained, referred to the energy level of QW1 and that of QW2.

This shows how the energy level of a T-QWR increases with reducing b. The energy level of a T-QWR gets closer to the energy level of QW1 or that of QW2 as b becomes smaller or larger, respectively. This is because the T-QWR state converges into QW1 or QW2 in the thin ($b \ll a$) and thick ($b \gg a$) limits, respectively, as demonstrated in figures 6 and 8. The slopes for the energy levels of T-QWRs and that for QW2 against b give the energy broadening induced by the monolayer fluctuation of the QW2 thickness b. The slope for the T-QWRs is smaller than that for QW2 with the same thickness b, showing that T-QWRs are less affected by b than QW2. Fitting the data points with a linear relation, SSA calculated the energy broadening of T-QWRs at $b = a$ to be 3.4 and 7.0 meV ML^{-1} for

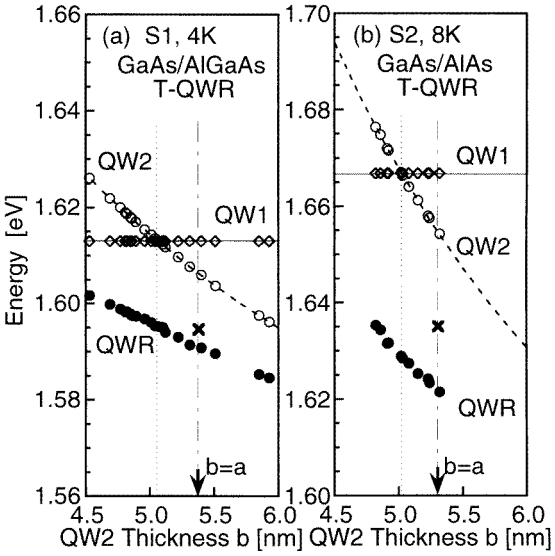

Figure 9. The energies of the PL peaks are shown by solid circles for QWRs, by blank diamonds for QW1, and by blank circles for QW2 in S1 (a) and S2 (b) as functions of the thickness of QW2, b. The broken curves show the energy level of QW2 calculated under the effective-mass approximation. The dotted lines indicate the energy level when the levels of QW2 and QW1 are identical. The chain lines indicate the situation in which the thickness b is identical to a. (Reproduced from reference [16].)

the two series. These two values seem quite reasonable, since the observed PL linewidth for T-QWRs corresponds to a fluctuation of about 2 ML.

3.3. 4 nm-scale $In_xGa_{1-x}As/Al_{0.3}Ga_{0.7}As$ T-QWRs

Then, SSA investigated $In_xGa_{1-x}As$ T-QWRs [23, 24]. The motivation for studying $In_xGa_{1-x}As$ T-QWRs was not only provided by the wish to achieve strong lateral confinement by decreasing the well energy, but also the wish to have more design flexibility and to establish a quantitative understanding of the lateral confinement energy in T-QWRs made of the new material system. The challenge lay in how to overcome the difficulty of growing $In_xGa_{1-x}As$ on a (110) surface [95] and that of fabricating high-quality $In_xGa_{1-x}As$ T-QWRs.

Figure 10 shows the PL spectra at 4 K of 4 nm-scale $In_{0.09}Ga_{0.91}As/Al_{0.3}Ga_{0.7}As$ T-QWR samples, with identical QW1 thickness $a = 4.1$ nm and different QW2 thicknesses $b = 3.5$, 3.9, and 4.4 nm [23].

The fabrication procedure for the samples was as follows. On a semi-insulating (001) GaAs substrate, SSA successively grew a 500 nm GaAs buffer layer, a 5 μm $Al_{0.3}Ga_{0.7}As$ layer, ten periods of $a = 4.1$ nm-thick $In_{0.09}Ga_{0.91}As$ multiple QWs and $c = 100$ nm-thick $Al_{0.3}Ga_{0.7}As$ barriers for QW1, a 10 nm AlAs layer, a 5 μm $Al_{0.3}Ga_{0.7}As$ layer, a 10 nm AlAs layer, and a 500 nm GaAs cap layer, by the conventional MBE method at a constant substrate temperature T_s of 560 °C, for a V/III flux ratio of ∼2, and at a GaAs growth rate of 0.7 μm h^{-1}. On the (110) surface of this wafer cleaved *in situ*, they subsequently grew at $T_s = 430$ °C an $In_{0.09}Ga_{0.91}As$ layer of thickness b for QW2, and a 2 ML-thick $Al_{0.3}Ga_{0.7}As$ cover layer, then at $T_s = 500$ °C a 10 nm-thick $Al_{0.3}Ga_{0.7}As$ barrier layer, and

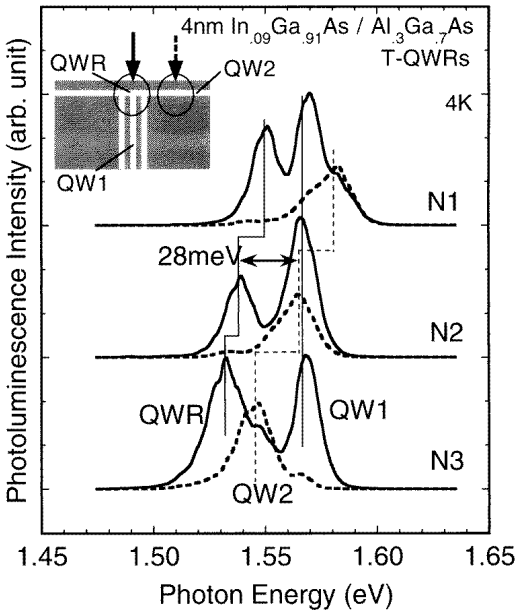

Figure 10. The spatially resolved PL spectra of three 4 nm-scale $In_{0.09}Ga_{0.91}As/Al_{0.3}Ga_{0.7}As$ T-QWR samples with identical QW1 thickness a and different QW2 thicknesses b measured from above the (110) CEO surface at 4 K with 633 nm excitation light from a He–Ne laser. Solid curves show the PL spectra for the 1 μm-wide region on QW1 and the QWRs, while the dashed curves show those for the 5 μm-wide regions of QW2. (Reproduced from reference [23].)

a 10 nm-thick GaAs cap layer. The V/III flux ratio was 30, and the $In_{0.09}Ga_{0.91}As$ growth rate was 0.5 μm h^{-1}. The growth conditions for the $In_xGa_{1-x}As$ on the (110) surface were optimized by means of repeated test growths and characterization, which was essential for the fabrication of the $In_xGa_{1-x}As$ T-QWRs [95]. Three samples were formed with the same initial growth procedure and three different CEO runs, varying the parameter b around 4 nm.

The solid and dashed curves in figure 10 show the PL spectra for the region on QW1 and the region on QW2, respectively, in which PL peaks assigned to QW1, QW2, and the QWRs have been observed. The precise energy of each structure has been determined from these spectra. From the observed peak energies, E^*_{1D-2D} for the three samples was determined: 19 meV, 28 meV, and 15 meV. It reached a maximum of 28 meV for the sample for which the PL energies of QW1 and QW2 are equal. The spectral linewidths of the three PL peaks were 15 meV, 20 meV, and 15 meV for QW1, QW2, and the QWR, respectively.

Figure 11 shows the PL spectra of a 3.5 nm-scale $In_{0.17}Ga_{0.83}As/Al_{0.3}Ga_{0.7}As$ T-QWR sample, with QW1 thickness $a = 3.7$ nm and QW2 thickness $b = 3.4$ nm [23]. The fabrication procedure was similar to that for the previous samples. The PL result was also similar to that shown in figure 10, but the large effective lateral confinement energy $E^*_{1D-2D} = 34$ meV was realized because of the stronger confinement. The spectral linewidths of the three PL peaks were 13 meV, 17 meV, and 14 meV for QW1, QW2, and the QWR, respectively, showing the smoothness of the hetero-interfaces.

It is important that a large value of E^*_{1D-2D}, 34 meV in this case, is achieved without introducing AlAs barriers, since the AlAs barrier has some drawbacks, especially as regards making QWR lasers [9, 33]. If an AlAs barrier is used to confine electrons, firstly separately

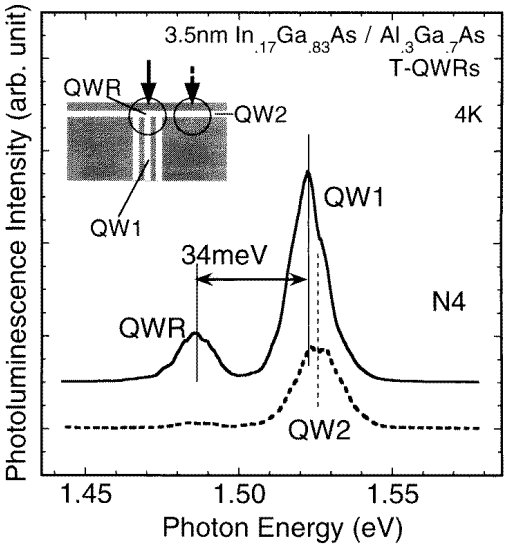

Figure 11. The spatially resolved PL spectra of a 3.5 nm-scale $In_{0.17}Ga_{0.83}As/Al_{0.3}Ga_{0.7}As$ T-QWR sample measured from above the (110) CEO surface at 4 K with 633 nm excitation light from a He–Ne laser. Solid curves show the PL spectra for the 1 μm-wide region on QW1 and the QWRs, while the dashed curves show those for the 5 μm-wide regions of QW2. (Reproduced from reference [23].)

confined heterostructures are not possible, second, the *in situ* cleavage and layer-by-layer growth are rather difficult with AlAs, and AlAs is easily oxidized and degraded, compared with $Al_{0.3}Ga_{0.7}As$, and third, to further increase E^*_{1D-2D}, we have more design flexibility left with $In_xGa_{1-x}As$, whereas further reduction of the QW thickness in GaAs/AlAs QWs results in type II structure, in which electrons are stabilized in the X valleys of the AlAs.

Table 1. A summary of the experimental results for four kinds of T-QWR sample: the effective lateral confinement energy of excitons E^*_{1D-2D} which is maximized when QW1 and QW2 have the same PL energy, the quantization energy E_Q given as the PL energy measured from the bulk band-gap energy in the QWs, and the band-gap discontinuity ΔE_g. (Reproduced from reference [23].)

	(Unit)	Reference [23]	Reference [23]	Reference [16]	Reference [16]
a (nominal)	(nm)	3.5	4	5	5
In content in well	(%)	17	9	0	0
Al content in barrier	(%)	30	30	30	100
E^*_{1D-2D} (maximum)	(meV)	34	28	18	38
E_Q	(meV)	176	146	94	148
ΔE_g	(meV)	557	464	374	1590
Ratio E^*_{1D-2D}/E_Q	(%)	19	19	19	26

Table 1 gives [23] a summary of the effective lateral confinement energy of excitons E^*_{1D-2D} which is maximized for QW1 and QW2 having the same PL energy, the quantization energy E_Q given as the PL energy measured from the bulk band-gap energy in the QWs, and the band-gap discontinuity ΔE_g, for the four kinds of T-QWR sample discussed above.

It is meaningful to consider the ratio E^*_{1D-2D}/E_Q shown in the table. In the infinite-barrier and constant-isotropic-effective-mass approximation, E^*_{1D-2D}/E_Q in balanced ($a = b$) T-QWRs should be constant (17% for the tentatively assumed electron mass of $0.067m_0$ and hole mass of $0.4m_0$) without excitonic effects, since all of the single-particle energy levels are proportional to the inverse square of the wave-function size. The ratio for two $In_xGa_{1-x}As/Al_{0.3}Ga_{0.7}As$ T-QWRs and a $GaAs/Al_{0.3}Ga_{0.7}As$ T-QWR is about 19%, close to the value 17%, while that for a GaAs/AlAs T-QWR can be as large as 26%. The high value of the ratio E^*_{1D-2D}/E_Q of 26% is attributable to the enhanced excitonic effect in tightly confined T-QWRs, which we discuss in the next section.

4. Exciton binding energy

Coulomb interaction of electrons confined in quantum structures leads to the realization of novel correlated states of fundamental interest in condensed-matter physics. Since quantum confinement forces electrons to interact strongly, the binding energy E_b of 2D excitons in QWs has been shown to increase, with reducing well thickness, to a value up to four times as large as the bulk value (4.2 meV for GaAs) [96], leading to room temperature excitonic absorption [97]. In QWRs, the excitonic effect is potentially further enhanced by laterally compressing the wave functions into the nanometre-scale regime [98, 99].

The evaluation of 1D exciton binding energy E_b was first carried out via PL-shift measurements under magnetic fields. In 1989, Kohl and co-workers [82] reported 15% enhancement of E_b compared with the value for the original 2D system, in QWRs formed by post-growth etching so as to have 14 nm $\times$ 70 nm cross-sectional size. Then, Nagamune and co-workers [46] reported $E_b = 10.1$ meV for V-groove QWRs (10 nm $\times$ 20 nm), analysing the measured shifts assuming an anisotropic hydrogen-like exciton model. We should note, however, that this analysis was useful for QWRs in the regimes of weak or centre-of-mass confinement, whereas it overestimates E_b for 1D excitons in the regimes of strong or individual confinement, as will be explained in section 6.

Rinaldi and co-workers [44] reported the 1D exciton binding energy E_b of their V-groove QWRs. Via a two-photon absorption measurement, E_b was obtained for both the ground and second-subband excitons: 10 and 8 meV, respectively. They obtained larger values of 12.5 and 10 meV from the analysis of magneto-PL measurements.

For T-QWRs, precise analysis of the PL energy of QWRs in comparison with that of QWs is possible, and can be used to determine the 1D exciton binding energy E_b. In 1993, Wegscheider and co-workers [9] reported enhancement of E_b by 7 meV for 7 nm-scale $GaAs/Al_{0.3}Ga_{0.7}As$ T-QWRs, which corresponds to about 50% enhancement from the value of E_b for the 7 nm-thick parent QWs.

Then, SSA systematically evaluated E_b for 1D excitons [16], by analysing the measured effective lateral confinement energies of excitons in a series of 5 nm-scale $GaAs/Al_{0.3}Ga_{0.7}As$ T-QWRs (S1) and 5 nm-scale GaAs/AlAs T-QWRs (S2), as already shown in figure 9. It is found that E_b is enhanced by 13 ± 3 meV for 5 nm-scale GaAs/AlAs T-QWRs, while the enhancement of E_b was only 3 ± 3 meV for 5 nm-scale $GaAs/Al_{0.3}Ga_{0.7}As$ T-QWRs; we investigate this in the following.

4.1. 5 nm-scale $GaAs/Al_{0.3}Ga_{0.7}As$ and GaAs/AlAs T-QWRs

Among the series of T-QWRs for which data are given in figure 9, SSA [16] examined the T-QWRs formed by two QWs with identical well thicknesses ($b = a$); these are called balanced T-QWRs. Note that balanced T-QWRs are the ones best suited to confine

electrons efficiently.

To analyse the energy levels of T-QWRs, SSA evaluated first the lateral confinement energy E_{1D-2D} of electrons by neglecting the Coulomb interaction and by using the single-band effective-mass approximation. The lateral confinement energy of holes is estimated to be small (1–2 meV) [13] for the balanced T-QWRs due to the heavy and anisotropic hole mass. Thus, one can obtain the energy level of T-QWRs by simply subtracting E_{1D-2D} for electrons from the energy level of QW2. The energies thus calculated, neglecting the Coulomb interaction, are denoted by two crosses in figure 9. Note that the measured PL energy is lower than the calculated energy by 4 meV for S1 and by 14 meV for S2. These discrepancies should be mostly attributed to the additional enhancement of the Coulomb effect of 1D excitons due to the lateral confinement.

In the evaluation of the enhancement of E_b for balanced T-QWRs, SSA estimated that the experimental errors caused by the broadening of the PL spectra were about ± 2 meV and the theoretical errors caused by the neglect of the contribution of the holes were -1 ± 1 meV. Therefore, they concluded that the additional enhancements of E_b due to the lateral confinement were 3 ± 3 meV for S1 and 13 ± 3 meV for S2. If E_b for 5 nm-thick GaAs QWs is assumed to be 14 meV as reported [96], the binding energy E_b of 1D excitons in balanced T-QWRs is concluded to be 17 ± 3 meV for S1, and 27 ± 3 meV for S2. Note that E_b for S1 is about 1.2 times the original 2D value, and that E_b for S2 is about twice the original 2D value, or about 6–7 times the bulk value.

We should note that the additional enhancement of E_b due to the lateral confinement is significant (13 meV) for S2, whereas it is rather small (3 meV) for S1. Since S1 and S2 have well thicknesses that are almost the same ($a = b = 5.3$–5.4 nm), the difference in the enhancement of E_b is due to the barrier height difference, indicating the importance of very tight confinement.

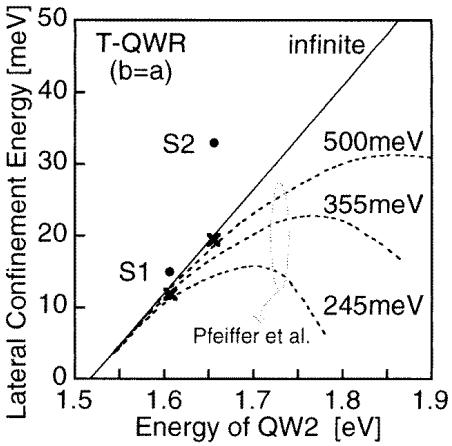

Figure 12. The lateral confinement energy in T-QWRs formed by two QWs with identical well thicknesses is shown as a function of the energy of QW2. The effective lateral confinement energy of excitons (E^*_{1D-2D}) shown by solid circles is compared with the lateral confinement energy E_{1D-2D} of electrons (the broken or solid lines) for 245, 355, 500 meV, and infinite barriers, calculated by Pfeiffer *et al*. (Reproduced from reference [16].)

To confirm this evaluation, SSA plotted (see figure 12) the lateral confinement energies as a function of the PL energy of QW2 [16]. Two solid circles represent the effective lateral confinement energies E^*_{1D-2D} measured for the balanced T-QWRs of series S1 and S2. For

comparison, they showed (see the solid and broken lines in figure 12) the theoretical lateral confinement energy E_{1D-2D} of electrons, which was calculated by Pfeiffer *et al* for the barrier heights of 245, 355, 500 meV, and infinity [13]. Also shown (by crosses) are the theoretical values of E_{1D-2D} for electrons calculated for the samples. Note in figure 12 that the calculated E_{1D-2D} for electrons increases linearly when the barrier height is infinite, and that E_{1D-2D} is proportional to E_Q, but rises only sublinearly with the energy of QW2 when the barrier height is finite. The experimental data indicated by solid circles, however, show a superlinear dependence, which indicates that the Coulomb interaction becomes increasingly important.

In the case of infinite barriers, both the energy level of the balanced T-QWRs and that of QW2 are scaled with b^{-2}. As a result, E_{1D-2D} for electrons is scaled with the energy level of QW2, which gives the linear dependence shown in figure 12. For finite barriers, the proportion of wave-function penetration into barriers becomes larger for QWR than for QW2 in the strong-confinement regime, so a sublinear dependence is obtained. In the weak-confinement regime, however, all of the energy levels are approximately scaled with the energy level of QW2, since the difference in wave-function penetration into barriers is negligible.

Note in figure 12 that the theoretical values for E_{1D-2D} for electrons represented by two crosses are very close to the solid line. This means that these balanced T-QWR samples are still in the regime where the scaling law should hold well. Thus, the contribution of the confinement energy without the Coulomb effect to E^*_{1D-2D} should be proportional to the energy level of QW2. Hence, the observed superlinear dependence of E^*_{1D-2D} is clear evidence of the substantial enhancement of the Coulomb interaction in 1D excitons when they are tightly confined in QWR structures.

5. Bloch wave functions—optical anisotropy

Optical anisotropy, i.e. the polarization dependence of the optical absorption and/or emission, has been one of the main subjects of interest in QWR studies, because it directly reflects the Bloch part of the wave function inherent to each quantum structure. In GaAs, the optical anisotropy is caused mainly by the anisotropic hole states at the tops of the valence bands, which each have a total angular momentum of $j = 3/2$. According to the lateral confinement in QWRs, mixing or splitting of the $j = 3/2$ valence band occurs, so the optical anisotropy described below is expected to be observed.

In Bastard's notation [3], neglecting spin indices, the conduction-band Bloch function is expressed as $|S\rangle$, whereas the valence-band Bloch function $|v\rangle$ is expressed as a linear combination of $|X\rangle$, $|Y\rangle$, and $|Z\rangle$, i.e. as $|v\rangle = C_x|X\rangle + C_y|Y\rangle + C_z|Z\rangle$. Since the PL intensity I_x with x-polarization is proportional to the optical transition matrix element $|\langle S|x|v\rangle|^2$, the intensity I_x gives $|C_x|^2$.

Disregarding the crystal anisotropy for simplicity, the heavy-hole (HH) and light-hole (LH) states in QWs grown in the z-direction are the Bloch states

$$|v\rangle_{QW,HH} = \frac{1}{\sqrt{2}}(|X\rangle \pm \mathrm{i}|Y\rangle)$$

$$|v\rangle_{QW,LH} = \sqrt{\frac{2}{3}}|Z\rangle - \frac{1}{\sqrt{6}}(\pm|X\rangle + \mathrm{i}|Y\rangle)$$

with the z-components of the angular momentum $j_z = \pm 3/2$ and $\pm 1/2$, respectively. Since x (z) is parallel (perpendicular) to the QW, the relative optical transition intensities are

calculated as 0, 3, 4, and 1 for $I_{\perp,\mathrm{HH}}$, $I_{\parallel,\mathrm{HH}}$, $I_{\perp,\mathrm{LH}}$, and $I_{\parallel,\mathrm{LH}}$, respectively. For HHs, $I_z/I_x = I_\perp/I_\parallel = 0\%$, while $I_y/I_x = I_\parallel/I_\parallel = 100\%$.

On the other hand, in ideal QWRs aligned along z with symmetric confinement, the lower-energy HH states and the higher-energy LH states become

$$|v\rangle_{\mathrm{QWR,HH}} = \sqrt{\frac{2}{3}}|Z\rangle - \frac{1}{\sqrt{6}}(\pm|X\rangle + \mathrm{i}|Y\rangle)$$

$$|v\rangle_{\mathrm{QWR,LH}} = \frac{1}{\sqrt{2}}(|X\rangle \pm \mathrm{i}|Y\rangle)$$

conversely to the QW case. Thus, $I_x/I_z = I_\perp/I_\parallel = 25\%$ is expected for HHs.

Note that here we use the term HH (LH) in the sense that it has heavier (lighter) effective mass than the LH (HH) in the direction of confinement of the QWs and QWRs. Thus, the lowest-energy excitons in QWRs and QWs are those composed of HHs having lower optical transition energies than LHs due to the smaller quantization energy.

In 1989, Tsuchiya and co-workers [61] measured the polarization-dependent PLE of tilted-SL-barrier QWRs formed on a vicinal substrate by MBE. Strong anisotropy was observed both for HH excitons and LH excitons, and this was attributed to the lateral confinement of QWRs. In the same year, Tanaka and Sakaki [62] reported similar effects in a new type of QWR, grid-inserted QWs, grown on vicinal substrates by MBE. The corrected formulation for analysing these results was given by Sercal and Vahala (reference [100]). Much theoretical work has been reported using more realistic and improved models for various QWRs.

With investigations of the contribution of the lateral confinement, the polarization dependence of the PL and PLE spectra had been presented for most types of GaAs QWR structure [8, 28, 34, 61, 62, 64, 67, 69]. However, it was not easy to experimentally evaluate the optical anisotropy introduced purely by the lateral confinement in QWRs (references [100–102]).

This is firstly because optical anisotropy is also caused by the valence-band anisotropy due to the warping distortion, uniaxial strain, or anisotropic perturbation potential of the anisotropic interface roughness (reference [103]). In addition, for QWRs grown on patterned substrates, the anisotropy in the macroscopic sample geometry can induce additional polarization dependence of their PL and PLE spectra. Furthermore, for small QWRs below the 10 nm scale which are our current interest, the PL or PLE peaks tend to broaden and overlap with other spectral structures, which makes it difficult to quantify the optical anisotropy from the PL and PLE spectra. For quantitative analysis of the observed anisotropy, one must accurately characterize both the potential profile and the quantized energy levels of QWRs, which is often difficult.

For the T-QWRs and the parent QWs described in the previous sections, clear optical anisotropy has been observed experimentally. In the experiments described below [19, 20], the optical anisotropy induced by the lateral confinement in the T-QWRs was experimentally evaluated via the comparison between the observed optical anisotropy for the T-QWRs and that for the reference QWs. Furthermore, the confinement-induced optical anisotropy was traced for the T-QWRs with various QW2 thicknesses b, showing the 2D–1D–2D dimensional crossover in the effective lateral confinement energy $E^*_{\mathrm{1D-2D}}$.

As regards V-groove QWRs, recent PLE experiments have shown optical anisotropies of ground and higher subband transitions in very good agreement with theoretical calculations, owing to the improvement of the sample quality, the structure characterization, and the numerical calculation methods [42, 52].

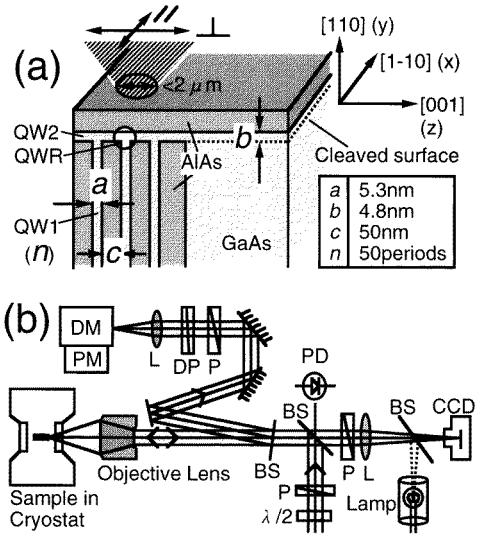

Figure 13. (a) The geometry of the structure, the crystal orientation, and the polarization, with the definition of the x-, y-, and z-directions, for the 5 nm-scale GaAs/AlAs T-QWR sample fabricated by the cleaved-edge-overgrowth method. (b) A schematic diagram of the micro-PL set-up. Key: DM: double monochromator; PM: photomultiplier; L: lens; P: polarizer; DP: depolarizer; PD: photo-diode; BS: beam-splitter; $\lambda/2$: half-wave retarder. (Reproduced from reference [19].)

5.1. 5 nm-scale GaAs/AlAs T-QWRs

We have already shown, in figure 4, the polarization-dependent PL and PLE spectra of the 5 nm-scale GaAs/AlAs T-QWR sample obtained by SSA [19]. Figure 13 shows a schematic diagram of the PLE measurement geometry and set-up. SSA defined [001] (the first growth direction) as the z-direction, [110] (the overgrowth direction) as the y-direction, and $[1\bar{1}0]$ (the wire direction) as the x-direction. They denoted polarization along x (z) as $\parallel$ ($\perp$), since x (z) is parallel (perpendicular) to the T-QWRs and the QW1 layers.

In the PLE spectra, the large PLE structures above 1.66 eV are due to the HH and LH excitons in QW1. The optical anisotropy of QW1 agrees well with the well-known optical anisotropy of standard (001) QWs observed from the (110)-cleaved surface (reference [104]). The forbidden transition of HHs with $\perp$ polarization was weakly observed. The observed PLE intensity $I_{\perp,\mathrm{HH}}$ for QW1 was about 14% of $I_{\parallel,\mathrm{HH}}$, in fair agreement with the PL data, which gave $I_\perp/I_\parallel = 6\%$.

As regards QWRs, figure 4 shows the PLE signal ratio $I_\perp/I_\parallel \simeq 39\%$. Since there is some contribution of the smearing tail structures of QW1 and the stray light, the estimation requires a proper extraction of these contributions. The value is obtained from the comparison of the peak intensity ratios, because peak heights are least affected by the additional contribution of the tail structures. The value is in fair agreement with the PL value of $I_\perp/I_\parallel \simeq 20\%$.

To look into the optical anisotropy of QWRs, we need to compare the data with those for the reference QW on a (110) surface to separate out the optical anisotropy due to the crystallographic anisotropy (reference [105]). For the reference GaAs/$Al_{0.3}Ga_{0.7}$As QW of 5.4 nm thickness formed on a (110) surface, the signal ratio $I_\perp/I_\parallel$ was 60% at the PL peaks, and was 67% in the PLE; these values show good agreement with each other.

Table 2. The optical anisotropy $I_\perp/I_\parallel$—that is, $I_{[001]}/I_{[1\bar{1}0]}$—for heavy-hole exciton transitions in T-QWRs, the reference (110) QW, and QW1 evaluated via PL, PLE, and theories assuming anisotropic and isotropic valence-band structures. (Reproduced from reference [19].)

Sample	PLE (%)	PL (%)	Theory (%) (anisotropic)	Theory (%) (isotropic)
QWR	39	20	34	25
(110) QW	67	60	86	100
QW1	14	6	0	0

The results on the optical anisotropy obtained are summarized in table 2. Although the values of $I_\perp/I_\parallel$ tend to be smaller for the PL data than for the PLE data, we found a clear difference between the results for the QWR and the reference (110) QW, which is ascribed to the optical anisotropy resulting purely from the lateral confinement in QWRs.

For the simplest model, with axial symmetry along the x-direction, neglecting the crystal-band anisotropy and the asymmetric shape of the QWR, we obtain $I_\perp/I_\parallel = 25\%$ for QWRs, and $I_\perp/I_\parallel = 100\%$ for the reference (110) QW. When the crystal-band anisotropy is taken into account under the approximation of infinite barriers and cylindrical shape (references [106, 107]), the optical anisotropy ratio $I_\perp/I_\parallel$ is 34% for the QWR, whereas for the reference (110) QW it is $I_\perp/I_\parallel = 86\%$. These values are compared with the experimental results in table 2. In spite of the obvious difference in shape between cylindrical rods and the T-QWRs, we find a good agreement between the model calculation results and the experimental ones.

5.2. 5 nm-scale GaAs/$Al_{0.3}Ga_{0.7}$As T-QWRs

Next, SSA [20] discussed the confinement-induced optical anisotropy traced for the T-QWRs with various QW2 thicknesses b showing the 2D–1D–2D dimensional crossover in the effective lateral confinement energy E^*_{1D-2D}. The T-QWR samples studied here were the series of 5 nm-scale GaAs/$Al_{0.3}Ga_{0.7}$As T-QWRs used in the above-mentioned study of lateral confinement energy and exciton binding energy (figures 5, 6, and 9).

Figure 14 shows the spatially resolved polarization-dependent PL spectra of four GaAs/$Al_{0.3}Ga_{0.7}$As T-QWR samples with identical QW1 thickness $a = 5.4$ nm and different QW2 thicknesses $b = 4.8$ nm, 5.3 nm, 5.9 nm, and 8.1 nm. Solid (dashed) curves show the PL intensity $I_\parallel$ ($I_\perp$) with the polarization parallel (perpendicular) to the T-QWRs and the QW1 layers. Thick (thin) curves show the PL for the region with T-QWRs (a 5 μm-wide QW2) indicated by a thick (thin) arrow in the inset.

The PL spectrum of each sample has three peaks, which are assigned to the lowest-energy excitons in T-QWRs, QW2, and QW1. The effective lateral confinement energy E^*_{1D-2D} of excitons in these T-QWRs with various values of b are plotted in figure 15(a), which is basically the same as figure 6, but for a wider range of b.

It is to be stressed that E^*_{1D-2D} represents the dimensionality of the excitons confined in T-QWRs: E^*_{1D-2D} reaches its maximum at $b = 5.1$ nm, where the energy levels of QW1 and QW2 are the same, indicating that a well-stabilized 1D state is realized; E^*_{1D-2D} decreases and approaches zero as the thickness b is decreased or increased away from 5.1 nm. The decrease in E^*_{1D-2D} demonstrates how the T-QWR states deviate from the well-stabilized 1D state and take on a 2D character. When the energy difference between QW1 and QW2 is so large that E^*_{1D-2D} is close to zero, the influence of the higher-energy QW can be regarded

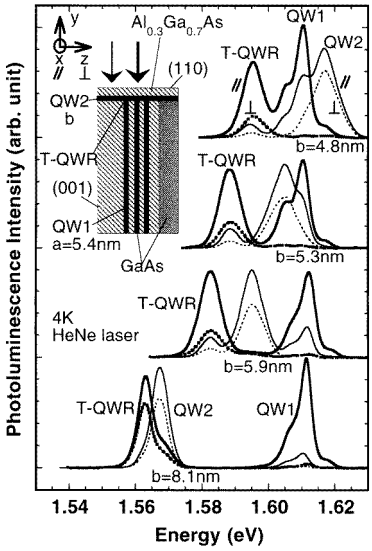

Figure 14. Spatially resolved polarization-dependent PL spectra measured at 4 K for four kinds of GaAs/$Al_{0.3}Ga_{0.7}As$ T-QWR sample. The inset shows a schematic diagram of the structure of the T-QWR samples. Solid (dashed) curves show the PL intensity with polarization parallel (perpendicular) to the T-QWRs and the QW1 layers. Thick (thin) curves show the PL for the region with T-QWRs (a 5 μm-wide QW2) indicated by a thick (thin) arrow in the inset. (Reproduced from reference [20].)

as a weak perturbation. In such regions, the T-QWR state is almost 2D-like. Hence, it is concluded that the 1D–2D dimensional crossover is observed via the effective lateral confinement energy E^{*}_{1D-2D} for T-QWRs with various values of b, shown in figure 15(a).

Note in figure 14 that strong polarization anisotropy is observed in the PL of the T-QWR, QW1, and QW2. The PL intensities with parallel polarization shown by solid curves were at all times larger than the PL intensities with perpendicular polarization shown by dashed curves. The optical anisotropies $I_{\perp}/I_{\parallel}$ for the QWRs, QW1, and QW2 for various samples with different values of b are plotted in figure 15(b). Although some data are scattered, the optical anisotropies for QW1 and QW2 are close to the predicted values of 0% and 86%, respectively (references [106, 107]).

On the other hand, the optical anisotropy $I_{\perp}/I_{\parallel}$ for T-QWRs increases with b from a value close to that for QW1 to a value identical to that for QW2. These results are interpreted in terms of the 2D–1D–2D dimensional crossover from QW1, via well-stabilized QWRs, to QW2, observed as the change in the confinement-induced valence-band anisotropy in T-QWRs.

As shown in table 2, the theory including the crystal anisotropy (references [106, 107]) gives the following values. For QW1 with confinement in the z-direction, $I_{\perp}/I_{\parallel} = 0\%$. For ideal QWRs with confinement symmetric around the x-direction, we expect $I_{\perp}/I_{\parallel} = 34\%$. For QW2 with confinement in the y-direction, we expect $I_{\perp}/I_{\parallel} = 86\%$. Therefore, as b is increased from zero to $b \gg a$, we expect that $I_{\perp}/I_{\parallel}$ should vary from 0%, passing through 34% when the confinement in the two directions is balanced, to 86%. This theoretical prediction is in good agreement with the experimental result shown in figure 15(b). The observed increase of $I_{\perp}/I_{\parallel}$ with b shows the increased $|Z\rangle$-component and the simultaneous change in the $|X\rangle$-component in the valence-band Bloch functions of T-QWRs with the

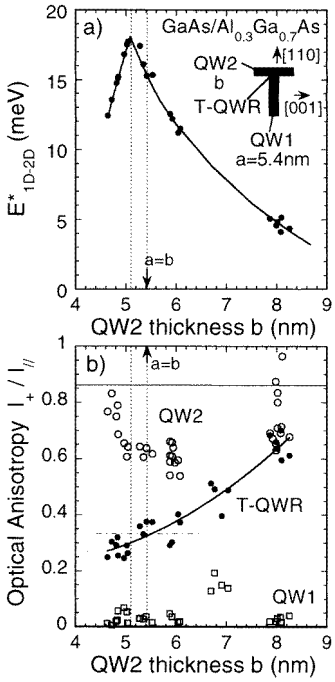

Figure 15. (a) The effective lateral confinement energy E^*_{1D-2D}, defined as the difference between the lowest 1D exciton energy in T-QWRs and the lowest 2D exciton energy in QW1 and QW2, plotted against the QW2 thickness b. The vertical broken lines are drawn at $b = a = 5.4$ nm where the thicknesses of QW1 and QW2 are equal, and at $b = 5.1$ nm where the PL energies of QW1 and QW2 are equal. The solid curve is drawn to guide the eye. (b) The optical anisotropy, defined as the PL peak intensity ratio $I_\perp/I_\parallel$ between the perpendicular and parallel polarizations, for T-QWRs (solid circles), QW1 (open squares), and QW2 (open circles) plotted against the thickness of QW2, b. The solid curve is drawn to guide the eye. The results are to be compared with the theoretically predicted values of 0%, 86%, and 34% for QW1, QW2, and the symmetric QWRs, respectively, which are shown by the horizontal lines. (Reproduced from reference [20].)

reduced confinement in the z-direction, which demonstrates the change in the valence-band anisotropy induced by the varied confinement under the dimensional crossover.

6. Envelope wave functions—magneto-PL

The lateral size of the exciton wave function in the effective-mass approximation, or the envelope part of the electron–hole relative wave function, can be evaluated by studying the energy shift of the PL under a magnetic field. When the Landau orbit is far larger than the exciton diameter, the effect of a magnetic field $\boldsymbol{B}$ is treated as perturbation. Then, a quadratic PL energy shift $\Delta E = \beta \boldsymbol{B}^2$ is expected for the weak magnetic fields $\boldsymbol{B}$ on the basis of second-order perturbation theory, which is useful as a measure of the effective size of the exciton wave functions.

With rotational symmetry in the exciton wave function around the magnetic fields $\boldsymbol{B}$ applied along the z-axis, the quadratic coefficient β is expressed as the diamagnetic coefficient $\beta = \langle e^2(x^2 + y^2)/8\mu \rangle$, where μ is the reduced mass of electrons and holes, and

$\boldsymbol{r} = (x, y, z)$ is the electron–hole relative coordinate for excitons (reference [108]). Thus, the effective area $\langle x^2 + y^2 \rangle$ and the effective diameter $d = \sqrt{\langle x^2 + y^2 \rangle}$ perpendicular to the magnetic field are obtained from β. In the cases of the lowest excitons in the bulk and QWs perpendicular to $\boldsymbol{B}$, the diamagnetic expression for β is correct. However, it holds only approximately for QWRs. Making this approximation (i.e. the diamagnetic approximation) is allowed when the lateral confinement is weak in the directions perpendicular to $\boldsymbol{B}$. The PL shifts under magnetic fields have been studied for various QWRs on the basis of the diamagnetic approximation.

In 1989, Kohl and co-workers [82] first reported a diamagnetic shift measurement on QWRs formed by post-growth etching, although these QWRs were rather wide (14 nm $\times$ 70 nm) and in the centre-of-mass-confinement regime. They concluded that the exciton binding energy E_b was enhanced by about 15% compared with that of the original 2D system because of the lateral confinement on a 70 nm scale.

In 1992, Nagamune and co-workers [46] reported a diamagnetic shift measurement on V-groove QWRs (10 nm $\times$ 20 nm). They determined the quadratic coefficients of the rather broad PL of QWRs by applying high magnetic fields up to 40 T. Analysing the quadratic coefficients for three directions as the diamagnetic coefficients, and assuming the anisotropic hydrogen-like 3D exciton model, they obtained $E_b = 10.1$ meV, which is larger than the bulk value. For the various QWRs so far reported on, the PL shifts under magnetic fields have been studied in a similar way [44, 45, 50, 65, 83].

However, there are some important points that we should not overlook if we wish to extend these experiments to QWRs in the strong-confinement regime.

We should first note that the reference measurement should be done with corresponding QWs instead of bulk, because the diamagnetic shift of 2D excitons in QWs is already smaller than that of 3D excitons in bulk (reference [109]). Since the Coulomb interaction is enhanced in QWs by the confinement in the normal direction, the diamagnetic shift of 2D excitons in QWs is already reduced from the bulk value. The Bohr radius of 2D excitons decreases substantially when the well thickness b is reduced, especially when it is reduced to below 10 nm. Hence, to probe into the lateral confinement effect in QWRs, it is essential to compare the diamagnetic shifts of QWRs with those of QWs having the same normal thickness.

Second, as the confinement becomes stronger, the diamagnetic shift becomes smaller, while the PL linewidth or the fluctuation of the energy level tends to be rather larger. This makes it difficult to examine smaller diamagnetic shifts with a sufficient accuracy. Hence, it is important to prepare very narrow QWRs with good uniformity having the spectrum linewidth.

Third, making the diamagnetic approximation is allowed only when the magnetic field $\boldsymbol{B}$ is applied perpendicularly to the plane of the weakest lateral confinement in the QWRs. Therefore, examination of the diamagnetic approximation is required—in particular, analysis of the quadratic coefficients β measured in all three directions.

Fourth, the estimation of the exciton binding energy on the basis of the anisotropic hydrogen-like 3D exciton model is useful for QWRs in the weak- or centre-of-mass-confinement regimes, whereas this is not appropriate for 1D excitons in the strong- or individual-confinement regimes. Such an analysis attributes the squeezing of the exciton wave function totally to the Coulomb interaction, and results in the overestimation of E_b. We should note that the 1D exciton binding energy is the binding energy of the Coulomb bound state of 1D electrons and holes measured from the free state of 1D electrons and holes which are free in one direction but still confined in two directions.

As a result of considering these points, SSA [15, 17, 18] organized two types of magneto-

PL experiment on T-QWRs in the strong-confinement regime. In the first experiment [15, 17], the quadratic PL shifts of the series of T-QWR samples with small linewidths were measured in comparison with those of reference QWs, where the magnetic field was applied in one direction perpendicular to the weakest-confinement plane. On the basis of the allowed diamagnetic approximation, the effect of lateral confinement on exciton wave functions in T-QWRs was quantitatively evaluated, separately from the enhanced 2D excitonic effect.

In the second experiment [18], the quadratic shifts were measured in all three directions. Since making the diamagnetic approximation is not allowed for all of the directions, the effect of confinement on the envelope wave functions is discussed taking into consideration the adequacy (or inadequacy) of the diamagnetic approximation, instead of estimating the exciton binding energy making the unjustified diamagnetic approximation and assuming the anisotropic hydrogen-like 3D exciton model to be appropriate.

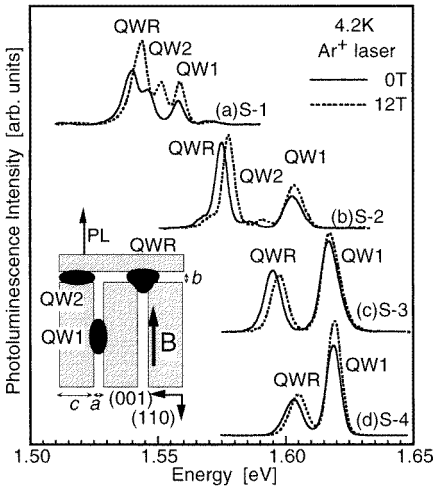

Figure 16. PL spectra measured at 4.2 K for the QWs (QW1 and QW2) and the QWR regions of four samples: (a) 9.8 nm × 11.6 nm, (b) 6.0 nm × 6.4 nm, (c) 5.2 nm × 5.3 nm, and (d) 5.2 nm × 4.9 nm. Solid lines are for zero magnetic field while dotted lines are for the field of 12 T. The basic structure of the T-QWRs is shown in the inset, where QW1, QW2, and the QWR are also defined. (Reproduced from reference [15].)

6.1. 5–10 nm-scale GaAs/$Al_{0.3}Ga_{0.7}$As T-QWRs with $\boldsymbol{B}$-fields parallel to one axis

A magneto-PL experiment was performed by SSA [15, 17] on four GaAs/$Al_{0.3}Ga_{0.7}$As T-QWR samples. The geometry parameters (cf. figure 13) of the various samples were as follows: $a = 9.8$ nm, $b = 11.6$ nm, $c = 200$ nm, and $n = 35$ for the first sample (denoted as 9.8 nm × 11.6 nm); $a = 6.0$ nm, $b = 6.4$ nm, $c = 100$ nm, and $n = 50$ for the second (denoted as 6.0 nm × 6.4 nm); $a = 5.2$ nm, $b = 5.3$ nm, $c = 31$ nm, and $n = 200$ for the third (denoted as 5.2 nm × 5.3 nm); and $a = 5.2$ nm, $b = 4.9$ nm, $c = 31$ nm, and $n = 200$ for the fourth (denoted as 5.2 nm × 4.9 nm). Since the energy level of QW1 is set close to, but always higher than, that of QW2 for all samples, the confinement of the QWR state is slightly stronger along the [110] (normal) direction than that along the [001] (lateral) direction. Therefore, the diamagnetic approximation is useful when the magnetic

field is applied along the [110] axis. Such a geometry was adopted in this magneto-PL experiment, as described below.

PL spectra of each sample were measured through an optical fibre with a 100 μm core diameter, which was attached to the (110) CEO surface of the sample in the geometry shown in the inset in figure 16. The sample was directly immersed in liquid helium, and placed in the bore of a superconducting magnet to apply a magnetic field up to 12 T perpendicularly to the (110) surface. The sample mounted on the fibre was then excited by an Ar^+ laser. PL from the sample was collected through the same fibre, and was dispersed into a 0.32 m grating monochromator.

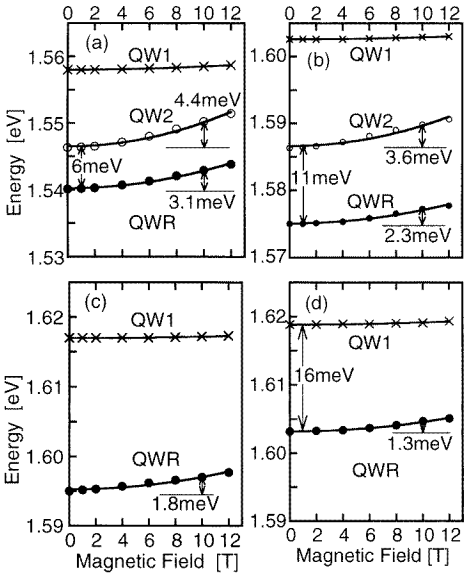

Figure 17. Diamagnetic shifts of various PL peaks from four samples: (a) 9.8 nm × 11.6 nm, (b) 6.0 nm × 6.4 nm, (c) 5.2 nm × 5.3 nm, and (d) 5.2 nm × 4.9 nm. We also show diamagnetic shifts at 10 T, which are determined by fitting the data points with a parabolic relation. (Reproduced from reference [15].)

The solid lines in figure 16 are PL spectra of the four samples measured at 0 T. Note that all of the peaks are clearly observed with linewidths of 4–7 meV, indicating the good uniformity of the structures. When magnetic fields were applied, all of the PL peaks shifted towards higher energy, as shown by dashed lines in figure 16. SSA plotted (see figure 17) the positions of all of the PL peaks as a function of the magnetic field $\boldsymbol{B}$. Note that the amount of shift is only a few to several meV even at 12 T. All of the data are well fitted by parabolic relations for the low magnetic fields as shown by the solid lines. The coefficient β is found to have the values 31, 23, 18, and 13 μeV T^{-2} for the four samples.

In figure 18, we reproduce the figure in which SSA plotted (as solid circles) the diamagnetic coefficients β of four QWRs as a function of the well thickness b of QW2. The scale of d is deduced from the assumed reduced mass $\mu = 0.058m_0$. For comparison, SSA collected the coefficients β of nine GaAs/$Al_{0.3}Ga_{0.7}$As QWs having different well thicknesses b, and plotted them too (as blank circles and blank squares). The blank circles are for QWs grown on (110) substrates, while blank squares are for QWs on (001) substrates. The data points for the 11.6 nm-thick QWs and 6.4 nm-thick QWs are for QW2 for the first two samples.

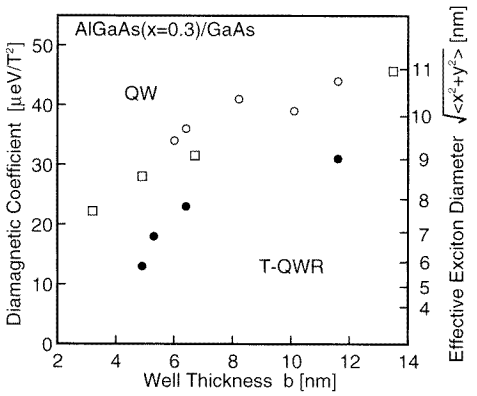

Figure 18. The diamagnetic coefficients of the four T-QWRs (solid circles) and nine $GaAs/Al_{0.3}Ga_{0.7}As$ QWs. The blank circles are for QWs grown on (110) substrates, while blank squares are for QWs on (001) substrates. (Reproduced from reference [15].)

It should be first pointed out that in figure 18 the diamagnetic coefficients β of QWs get smaller as the well thickness b is reduced, and that the coefficients β of the four QWRs are all substantially smaller than those of the corresponding QWs.

As regards the QWs, the reduction of β, or the effective area of the excitons, is caused by the enhanced Coulomb interaction between the 2D electrons and holes, which is reflected also in the enhancement of the exciton binding energy. As b is reduced, and as the confinement in the normal direction becomes stronger, β gets smaller, going from the bulk value to the 2D quantum limit value: for the bulk, $\beta_{3D} = e^2a_B^2/4\mu = 109\ \mu\text{eV T}^{-2}$ and $d_{3D} = \sqrt{2}a_B = 16.9$ nm; for the 2D quantum limit, $\beta_{2D} = (3/16)e^2a_B^2/4\mu = 20\ \mu\text{eV T}^{-2}$ and $d_{2D} = (\sqrt{3}/4)d_{3D} = 7.3$ nm. Here, two GaAs parameters, the effective Bohr radius a_B of 12 nm and the reduced mass of 0.058 m_0, were used.

By comparing the values of β or d for T-QWRs with those for QWs with the same value of b, we can evaluate the effect of lateral confinement separately from the confinement just along the normal direction, which enhances the 2D excitonic effect. For example, for the 9.8 nm $\times$ 11.6 nm sample, the effective exciton diameter d is 10.7 nm for QWs, but it is slightly reduced to 9.0 nm for QWRs because of its lateral confinement. For the 6.0 nm $\times$ 6.4 nm sample, d for QWs is reduced to 9.7 nm whereas d for QWRs is further squeezed to 7.7 nm. For the 5.2 nm $\times$ 4.9 nm sample, d for QWs is 8.6 nm but d for QWRs can become as small as 5.8 nm. These data clearly show that excitons are all laterally squeezed by the T-shaped potential profile in these QWR samples with feature sizes ranging from 5 nm to 12 nm.

The next point to be noted is that, in figure 18, β for QWRs in the 9.8 nm $\times$ 11.6 nm sample is still larger than those of very thin QWs ($b < 5$ nm). For this QWR, the introduction of the T-shaped potential is effective in confining the 2D exciton laterally, and reduces the effective diameter from 10.7 nm to 9.0 nm. However, the same level of squeezing is seen in 5 nm-thick QWs where the enhanced 2D excitonic effect reduces the exciton diameter. This again shows that the simple reduction of β or d is not always proof of lateral confinement.

The third point clarified by figure 18 is that the effective diameter of excitons in T-QWRs of the 5.2 nm $\times$ 4.9 nm sample is below the 2D quantum limit. Note that β is as small as 13 $\mu\text{eV T}^{-2}$ and d is squeezed to 5.8 nm. We must compare these values with those of 2D excitons. In the limit of thin QWs (the 2D quantum limit), β_{2D} is predicted

to get as small as 20 μeV T^{-2} and d shrinks to 7.3 nm. In reality, as the thickness of the wave function in GaAs QWs remains finite, one expects β to become saturated at around 22 μeV T^{-2} and $d = 7.6$ nm, which is indeed demonstrated for 3 nm-thick QWs. Therefore, it is concluded that the exciton wave function in the smallest T-QWR is squeezed more strongly than those of 2D excitons in GaAs QWs in the 2D quantum limit.

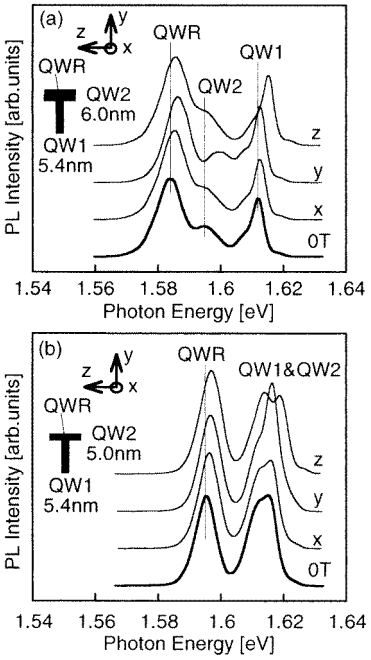

Figure 19. PL spectra measured at 4.2 K for two T-QWR samples with a QW1 thickness a of 5.4 nm and QW2 thicknesses b of 6.0 nm (a) and 5.0 nm (b). The solid lines are for zero magnetic field, while the fine lines are for the field of 12.5 T. Schematic diagrams of the structures of the T-QWRs are shown in the insets, where QW1, QW2, and the QWR are defined. The z-direction is defined as the first growth direction of [001], the y-direction as the second growth (overgrowth) direction of [110], and the x-direction as [1$\bar{1}$0], parallel to the QWRs. (Reproduced from reference [18].)

6.2. 5 nm-scale GaAs/Al$_{0.3}$Ga$_{0.7}$As T-QWRs with $\boldsymbol{B}$-fields parallel to three axes

In the next experiment, SSA studied [18] three 5 nm-scale GaAs/Al$_{0.3}$Ga$_{0.7}$As T-QWRs with the same QW1 thickness $a = 5.4$ nm and varied QW2 thicknesses b: 5.0 nm, 6.0 nm, and 7.6 nm. They define the z-direction as the first growth direction of [001], the y-direction as the second growth (overgrowth) direction of [110], and the x-direction as [1$\bar{1}$0], parallel to the QWRs, as shown in the insets of figure 19.

The solid line in figure 19(a) is the PL spectrum measured at 0 T for the sample having the QW2 thickness $b = 6.0$ nm. The PL peaks of the T-QWRs are sharp, with linewidths of about 8–10 meV.

For these samples, they applied magnetic fields $\boldsymbol{B}$ up to 12.5 T in the x-, y-, and z-directions, and measured the respective PL spectra. The three fine lines in figure 19(a) show the PL spectra with $B = 12.5$ T applied in the three directions, where all of the PL

peaks are blue-shifted from $B = 0$ T by different amounts.

They then measured the amount of shift ΔE as a function of the magnetic field $\boldsymbol{B}$, and found all of the peaks to show the quadratic dependence $\Delta E = \beta B^2$. The observed B^2-dependence shows that the magnetic field is to be considered as a weak perturbation for the excitons in T-QWRs.

Within the framework of second-order perturbation theory, β consists of the diamagnetic coefficient (reference [108]) and the Van Vleck paramagnetic coefficient. The diamagnetic term is a positive term proportional to the effective size of the excitons perpendicular to the magnetic field $\boldsymbol{B}$. The Van Vleck paramagnetic term is a negative term deduced from the second-order perturbation of the Zeeman term, proportional to $\boldsymbol{B}\cdot\boldsymbol{L}$, where $\boldsymbol{L}$ is the angular momentum of the excitons. In QWs, the Van Vleck paramagnetic term vanishes when the magnetic field is applied in the growth direction, because the lowest excitons must have rotational symmetry to have $\boldsymbol{L} = 0$. Therefore, the diamagnetic expression for β is correct as regards giving the effective size of the exciton wave functions in the plane normal to the magnetic field. For QWRs without rotational symmetry, it holds only approximately. Making the approximation (the diamagnetic approximation) is allowed when the lateral confinement is weak in the directions perpendicular to $\boldsymbol{B}$.

For other geometries of QWs and QWRs, the Van Vleck paramagnetic term is not negligible. Thus, the sizes of ΔE or β do not quantify the effective size of the exciton wave functions. On the other hand, it is safe to say that the value of β is reduced by the effect of lateral confinement, since the enhanced Van Vleck paramagnetic term is negative and the decreased diamagnetic term is positive. Therefore, the reduced ΔE or β qualitatively represents the magnitude of the lateral confinement.

It interesting to observe, in figure 19, the smallness of the shift of each PL peak. In figure 19(a), the shift of the PL peak for QW1 is large for $\boldsymbol{B} \parallel \boldsymbol{z}$ and small for $\boldsymbol{B} \parallel \boldsymbol{x}$ and $\boldsymbol{y}$, showing the expected feature that the wave function is spread in the xy-plane for QW1. In contrast, the shift of the PL peak for QW2 is large for $\boldsymbol{B} \parallel \boldsymbol{y}$ and small for $\boldsymbol{B} \parallel \boldsymbol{z}$ and $\boldsymbol{x}$, showing that the wave function is spread in the zx-plane for QW2. The shift of the PL peak for the QWR is largest for $\boldsymbol{B} \parallel \boldsymbol{y}$ and smallest for $\boldsymbol{B} \parallel \boldsymbol{x}$, showing that the confinement is tightest in the y-direction and least tight in the x-direction for the QWR state in the sample with $a = 5.4$ nm and $b = 6.0$ nm.

Figure 19(b) shows data for the sample with $a = 5.4$ nm and $b = 5.0$ nm. The shift of the PL peak for the QWR is now largest for $\boldsymbol{B} \parallel \boldsymbol{z}$ and smallest for $\boldsymbol{B} \parallel \boldsymbol{x}$, showing that the confinement is tightest in the z-direction for the QWR state, or that the QWR wave function tends to locate more in the QW1 region.

The least-squares-fitting analysis of the observed B^2-dependence for all of the samples has revealed a systematic change of β along the three axes for the varied QW2 thickness b, shown in figure 20. The figure demonstrates how the envelope wave function in T-QWRs varies according to the varied b, with constant a [18], in addition to the already discussed variation of the effective lateral confinement energy E^*_{1D-2D} and the optical anisotropy $I_\perp/I_\parallel$ observed in figure 15.

7. Oscillator strength

The oscillator strength of 1D excitons in QWRs has been one of the main subjects of investigation among the optical properties of semiconductor low-dimensional structures. Such study is particularly motivated by the expected concentration of oscillator strength into the lowest exciton state in QWRs as a result of the 1D electronic density of states (DOS) concentrated at the low-energy edge and the efficient Coulomb interaction among

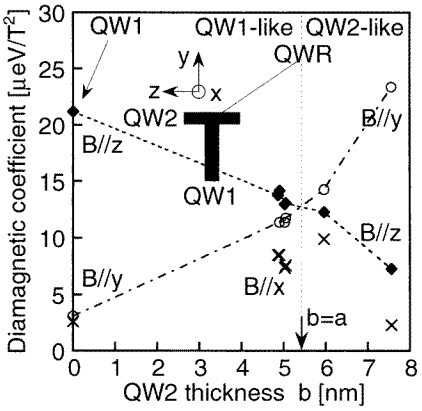

Figure 20. The quadratic coefficients β_x, β_y, and β_z in the quadratic energy shifts for the magnetic fields $\boldsymbol{B} \parallel \boldsymbol{x}$, $\boldsymbol{y}$, and $\boldsymbol{z}$ for QWRs are plotted as a function of the thickness of QW2, b; the β_x are shown by the crosses, the β_y by the open circles, and the β_z by the solid squares. (Reproduced from reference [18].)

the carriers that are tightly confined [98, 99].

For 2D excitons, Masumoto and co-workers (reference [110]) studied the oscillator strength of the lowest HH excitons in GaAs/AlAs QWs as a function of QW thickness by means of absorption measurements. The oscillator strength of the 2D excitons was substantially enhanced with decreasing QW thickness, showing the enhanced excitonic effect, while that of the 2D continuum of the lowest subband was constant.

The direct investigation of oscillator strength requires measurements of the absorption and/or reflection intensity, which, however, are difficult to carry out for QWRs because of the small volume of the QWR structures. To attack this problem within PL and PLE spectroscopy with higher sensitivity, careful study comparing systematic series of QWR samples is required, since we can only partly establish the relative intensities of the oscillator strength from these measurements.

Such measurements were attempted on QWRs formed by the CEO method. In 1996, Harris and co-workers [30] studied single strained QWRs formed by the CEO method by means of PLE using low-temperature near-field scanning optical microscopy. A factor-of-three oscillator strength enhancement for these QWRs compared to the QWs was concluded.

In the same year, SSA [21] studied the oscillator strength of the 1D exciton states using a series of T-QWR samples in which the lateral confinement was systematically changed. As shown below, it became enhanced and spatially concentrated with the increased lateral confinement. The absorption area intensity was about 50% higher for the lowest 1D excitons in $GaAs/Al_{0.3}Ga_{0.7}As$ T-QWRs formed by 5.2 nm- and 4.8 nm-thick QWs with the period of 36 nm than that in a reference 2D-like sample.

7.1. 5 nm-scale $GaAs/Al_{0.3}Ga_{0.7}As$ T-QWRs

Figure 21 shows [21, 22] the polarization-dependent PL and PLE spectra of three $GaAs/Al_{0.3}Ga_{0.7}As$ T-QWR samples, where the structure of QW1 is constant, with the well thickness $a = 5.2$ nm, the barrier thickness $c = 31$ nm, and the period $n = 200$, while the overgrown QW2 thickness b differs (4.8 nm, 6.9 nm, and 10 nm). The measurement was done via the (110) surface in the backward-scattering geometry for normal incidence.

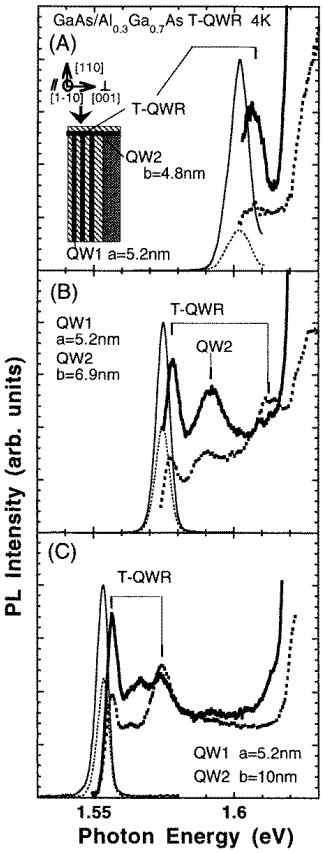

Figure 21. The PL (thin curves) and PLE (thick curves) spectra measured at 4 K for three $GaAs/Al_{0.3}Ga_{0.7}As$ T-QWR samples. While the well thickness of QW1, $a = 5.2$ nm, is constant, the well thickness of QW2, b, differs: $b = 4.8$ nm (A); $b = 6.9$ nm (B); $b = 10$ nm (C). The polarization of the light for detection in PL and excitation in PLE was parallel (solid curves) or perpendicular (broken curves) to the T-QWRs. The PLE intensities in (A)–(C) are normalized using identical large features due to the absorption at QW1 observed in all of the PLE spectra above 1.62 eV (not shown), and thus can be compared with each other. (Reproduced from references [21, 22].)

Thin curves show the PL spectra of the T-QWRs, and thick curves show their excitation spectra. Solid (broken) curves denote the polarization parallel (perpendicular) to the T-QWRs and the QW1 layers. The PLE intensities in figure 21(a)–21(c) are normalized using identical large features due to the absorption at QW1 observed in all of the PLE spectra above 1.62 eV (not shown) [21], and thus can be compared with each other.

Figure 21(A) shows the PL and PLE spectra of the T-QWRs with $b = 4.8$ nm, where the stable 1D exciton states are realized. The sharp PL linewidth of 8.5 meV, and the small Stokes shift of 4 meV indicate the good uniformity of the sample and the free-excitonic nature of the signals. Strong polarization dependence was observed, where the optical transition was more active for parallel polarization than for perpendicular polarization [19].

Figures 21(B) and 21(C) show the PL and PLE spectra of the T-QWRs with $b = 6.9$ nm and 10 nm, respectively, where the exciton states take on more 2D character close to QW2.

In fact, the polarization dependence of the PL becomes smaller and closer to that of QW2, as expected [20].

The PLE spectra in figure 21(B) show the HH and LH exciton peaks of the T-QWR at 1.578 eV and 1.613 eV, respectively. The peak at 1.592 eV shows a similar polarization dependence to that of the HH exciton in the T-QWR, and is ascribed to the HH exciton extending over the whole QW2 region.

Note that the PLE intensity of HH excitons in T-QWRs is comparable with that of QW2, where their area intensity ratio is about 1:2. This ratio is to be compared with the following geometrical factors. The period of the QWRs is given by $a + c = 36$ nm, in which the wave functions of 1D excitons in T-QWRs are bounded by the T-junction parts at a certain reduced lateral size. On the other hand, the 2D excitons denoted as QW2 are not bounded, but are extended over the period of 36 nm. Since the lateral size of a 1D exciton is less than 18 nm, the PLE area intensity ratio of 1/2 is larger than the geometrical size ratio for the 1D and 2D excitons.

Also note that the period of 36 nm is much smaller than the carrier diffusion length in QWs ($\sim\mu$m), so all of the carriers generated at QW2 are quickly captured into T-QWRs. In such a case, the PLE intensity is proportional to the absorption intensity, and their energy-integrated area intensities are proportional to the oscillator strength. Therefore, the enhanced and reduced PLE area intensities of T-QWRs and QW2 compared with the geometrical factors suggest that the oscillator strength of excitons in QW2 is transferred to those in T-QWRs.

The PLE spectra in figure 21(C) are very similar to those of QW2, composed of the HH exciton peak at 1.556 eV, the LH exciton peak at 1.574 eV which shows opposite polarization dependence to the HH exciton peak, and the flat region at 1.58–1.61 eV corresponding to the 2D-like DOS. The small features between the HH and LH exciton peaks are probably caused by the weak lateral modulation in the sample.

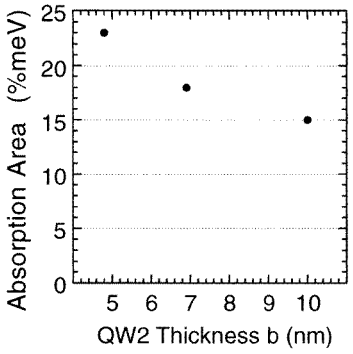

Figure 22. The enhancement of the absorption area intensity of HH excitons in T-QWRs with reduced QW2 thickness b, observed in samples with $b = 4.8$ nm (A), $b = 6.9$ nm (B), and $b = 10$ nm (C) (QW1 thickness: $a = 5.2$ nm; QWR period: $a + c = 36$ nm). Since lateral confinement is stronger for smaller b, the lateral size of the exciton wave function, and hence the cross-sectional area for the incident light, are smaller for smaller b. Thus, the local oscillator strength obtained by normalizing each datum with respect to the lateral size is significantly enhanced for smaller b. (Reproduced from reference [21].)

As regards the continuum state showing the 2D DOS of QW2, the absorption probability is known to be 1.3% (reference [110]). As already mentioned, all of the carriers absorbed by T-QWR and QW2 states are supposed to flow into the lowest exciton state in T-QWRs with

the same efficiency, and the PLE intensities of the T-QWR and QW2 are proportional to the absorption probability. Therefore, the absorption probability of 1.3% for the continuum state of QW2 is a useful standard in evaluating the absorption probability at T-QWRs, which we discuss below.

The central issue is the comparison of the PLE peak intensities among the figures 21(A)–21(C), especially for HH excitons in T-QWRs. Since the continuum state of QW2 in figure 21(C) shows the standard absorption probability of 1.3%, the peak absorption probabilities of HH excitons in T-QWRs in the three figures are then evaluated to be 2.7%, 2.9%, and 3.0%. Multiplying by the linewidth, we obtain the absorption area intensities of the three samples, which are 23% meV, 18% meV, and 15% meV, respectively, and are plotted in figure 22.

This shows that the oscillator strength is largest for T-QWRs with $b = 4.8$ nm, which is the case with the strongest lateral confinement among the three samples. Note that the lateral size of the exciton wave function is smallest in this sample, or, equivalently, that the cross-sectional area for the incident light is smallest, which should contribute to *reducing* the PLE intensity. That is to say, if we normalize the relative oscillator strength obtained with respect to the cross-sectional area for the incident light, we obtain significant enhancement of the local oscillator strength in T-QWRs with $b = 4.8$ nm. SSA concluded that the oscillator strength is not only enhanced, but also highly concentrated spatially in the T-junction part, when the lateral confinement is strong.

8. Lifetime

The purposes of the lifetime measurement of 1D excitons in QWRs were firstly to characterize the crystal quality in the QWRs as the non-radiative lifetime, and second to investigate the optical transition probability of 1D excitons as their radiative lifetime.

Many time-resolved PL measurements have been made on the exciton lifetime in QWRs formed by post-growth etching [74, 75]. A strong reduction of PL lifetime and a corresponding quenching of the PL intensity were found with decreased wire width due to side-wall non-radiative recombination. On the other hand, the PL lifetime of directly grown QWRs such as V-groove QWRs was found to be rather long due to the reduced non-radiative recombination. In 1992, Christen *et al* [38, 39] reported a CL decay time of 310 ps at 5 K for V-groove QWRs, and Miller *et al* [63] reported a PL decay time of 379 ps at 1.4 K for serpentine-SL QWRs, which were rather long compared with the values for reference QWs. These results evoked interest in the radiative decay process of 1D excitons.

To investigate the physics of the radiative decay process of 1D excitons, SSA and co-workers [55, 56] experimentally studied the temperature dependence of the PL radiative lifetime $\tau(T)$ in ridge QWRs grown on patterned substrates by MBE in 1994. It has been found that $\tau(T)$ for 1D excitons in the QWRs grows much more slowly, as $92\sqrt{T}$ ps $K^{-1/2}$, than that of 2D excitons in the reference QWs, given as $24T$ ps K^{-1}, resulting in a shorter 1D lifetime for $T > 20$ K. This unique temperature dependence was ascribed to the ineffective thermalization due to the 1D DOS in QWRs. A similar experiment was reported by Gershoni and co-workers [29] on the strained QWRs formed by the CEO method.

Kono and co-workers [48] studied the low-temperature lifetime of excitons in V-groove QWRs with various sizes [47]. They ascribed the observed increase in lifetime for reduced QWR size to the effect of the coherence length and the wave-function penetration into the barriers.

We describe in the following the experiments with the ridge QWRs and the analysis

based on theories of the radiative decay of 1D and 2D excitons, which suggest the importance of experiments at various temperatures.

8.1. Ridge QWRs

The temperature-dependent PL of excitons was measured for ridge QWRs and reference QWs, which are formed on top of ridge structures with two adjacent (111)B facets grown over a line-patterned GaAs(001) substrate by MBE [53, 54].

The patterned GaAs(001) substrate was prepared by photolithography and reactive-ion etching, and had line patterns of reverse-mesa structures along the [110] direction (1.6 μm width, 2 μm height, 4.0 μm period). Because of the crystallographic selectivity of epitaxy, the growth of a GaAs buffer on this substrate led to sharp ridge structures with two adjacent (111)B facets on top of the reverse mesas. On its top, Koshiba and co-workers deposited AlAs (barrier), GaAs (wire), $Al_{0.3}Ga_{0.7}As$ (barrier), and GaAs (cap) layers. TEM and SEM micrographs have shown that the ridge QWRs have crescent shapes of about 9 nm thickness and 18 nm width. In different regions on one wafer of the present QWR sample, non-uniformity of the initial mesa width had caused incomplete ridge structures with the (001) surface remaining at the top, on which QWs with 10 nm thickness and 120 nm width were formed. Koshiba and co-workers used these QWs (top-QWs) as the reference here.

They measured the time-resolved PL intensities excited by the second harmonics of yttrium lithium fluoride (YLF) laser pulses (526 nm, 5×10^9 photons cm^{-2}) with the time-correlated photon-counting method [55, 56].

To evaluate the lifetime of 1D and 2D excitons from these data, a least-squares fitting with an exponential decay was performed over a range of initial one-order-of-magnitude decay of the PL. Especially at lower temperatures, slow decay components most probably due to the localized exciton contribution are observed, as is generally the case with PL decay of ordinary QWs. However, one expects the initial one-order-of-magnitude decay to be dominated by the lifetime of free excitons except in the lowest-temperature region. The free-excitonic nature of the PL has also been confirmed by the small Stokes shifts in the PL and PLE measurements.

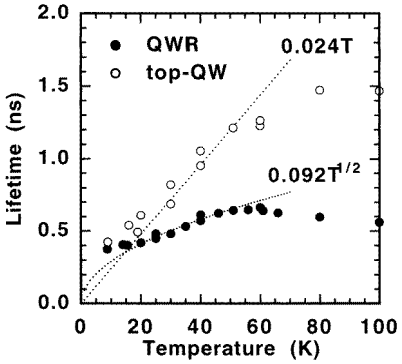

Figure 23. The temperature dependence of the PL decay time for ridge QWRs and top-QWs formed simultaneously by facet growth on a patterned substrate by MBE, excited by the second harmonics of YLF laser pulses. (Reproduced from reference [55].)

The values of the lifetime thus obtained are plotted against temperature in figure 23. We see that the lifetime of 2D excitons in top-QWs increases almost linearly with temperature,

which is usually observed for typical QWs, and is attributed to the behaviour inherent to the radiative lifetime of 2D excitons (references [111, 112]). This justifies the interpretation of the data for the present samples on the basis of the radiative lifetime of the excitons. If we compare the temperature dependence of the exciton lifetime in the QWRs with that of the top-QWs, the increase in the QWR lifetime is much weaker than that of the top-QWs.

This small temperature dependence of the 1D exciton lifetime $\tau(T)$ in QWRs is ascribed to the 1D DOS and the thermalization within it. Comparison with the following theories has revealed that $\tau(T)$ can be expressed as $92\sqrt{T}$ ps $K^{-1/2}$ for QWRs and as $24T$ ps K^{-1} for QWs.

8.2. Theoretical analysis

The 2D and 1D excitons in QWs and QWRs have direction(s) with translational symmetry in which they have a degree of freedom of translational motion, and other direction(s) without translational symmetry. The translational motion of excitons is specified by the centre-of-mass wave vector K. At finite temperatures, excitons are quasi-thermalized on the energy–dispersion curve $E = \hbar^2 K^2/2M$ (M is the exciton mass).

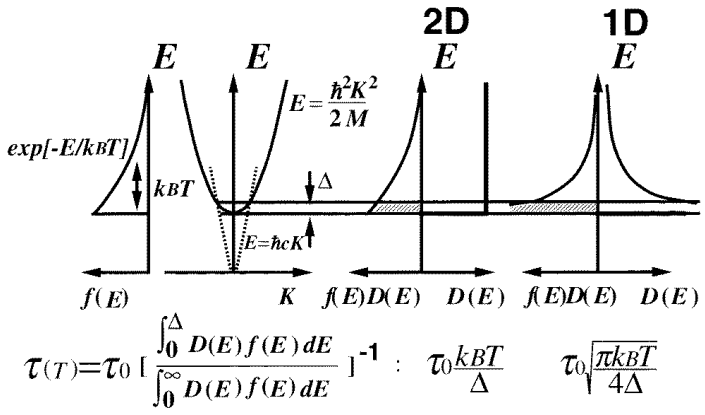

Figure 24. A schematic explanation of the thermalization of 2D and 1D excitons and their temperature-dependent radiative lifetime $\tau(T)$. The function $f(E)$ denotes the energy distribution function, assumed to be $\propto \exp(-E/k_BT)$ (a Maxwell–Boltzmann distribution), $D(E)$ denotes the DOS of the excitons, $\propto E^{-1/2}$ (=constant) for 1D (2D), Δ the maximum kinetic energy of excitons which can decay radiatively, and τ_0 the intrinsic radiative lifetime of the exciton at $K \sim 0$. The factor $\int_0^{\Delta} D(E)f(E)\,dE/\int_0^{\infty} D(E)f(E)\,dE$ shows the probability that the excitons are in the optically active region ($0 < E < \Delta$), and is indicated schematically as a hatched area. The integral is estimated by assuming $k_BT \gg \Delta$. (Reproduced from reference [56].)

In the optical transitions between the excitons and photons, the excitons with small wave vector $K < K_0$ are active, but those with large wave vector $K > K_0$ are inactive, where K_0 is the wave vector of light in the crystal with the same energy as the excitons. This is because of the rule of K-conservation in the direction of translational motion.

Thus, in the optical measurements like those of the absorption or PL, we detect signals only from the excitons with small wave vector $K < K_0$. Their lifetime is short because of their spatial coherence, and is characterized by the intrinsic radiative lifetime τ_0 of the $K = 0$ excitons. However, the excitons are in quasi-thermal equilibrium at finite temperatures, so the existence of the large-K excitons plays an important role in the understanding of their

dynamical properties. The lifetime observed is the average over those exciton states which are quasi-thermally distributed.

The averaged radiative lifetime $\tau(T)$ is given by [55, 56, 113]

$$\tau(T) \simeq \begin{cases} \tau_0\sqrt{\pi k_B T/4\Delta} & \text{(1D)} \\ \tau_0(k_B T/\Delta) & \text{(2D)} \end{cases} \tag{1}$$

for $T \gg \Delta/k_B \sim 1$ K ($\Delta = \hbar^2 K_0^2/2M$), where τ_0 is the intrinsic radiative lifetime of the exciton at $K \sim 0$, and the residual factor expresses the effect of thermalization to the optically inactive large-K states. The meaning of this factor is schematically shown in figure 24. Therefore, the radiative lifetime $\tau(T)$ is proportional to $\sqrt{T}$ for 1D, and proportional to T for 2D.

Following Hanamura's theory (reference [114]), we obtain the following expressions for τ_0 for the 1D and 2D excitons at $K = 0$ with polarization parallel to the wires and wells, respectively:

$$\tau_0^{-1} = \begin{cases} 6\pi^3(\lambda/a)\gamma_s & \text{(1D)} \\ 6\pi(\lambda/a)^2\gamma_s & \text{(2D)} \end{cases} \tag{2}$$

where λ is the wavelength of light, a is a phenomenological parameter in the 1D or 2D wave function assumed as $\propto \exp(-r/a)$, and γ_s is the contribution per unit cell to the band-to-band radiative decay rate.

In more probable cases (reference [111]), when the homogeneous broadening Δ^* of the excitons is so large that the uncertainty of the wave vector is comparable to K_0, it limits the spatial coherence of the excitons to the coherence length L^* ($\Delta^* \sim h^2/2ML^{*2}$). Then, the $K \sim 0$ exciton lifetime τ_0 is replaced by a longer lifetime τ_0^* limited by L^*, and the maximum wave vector K_0 of the optically active (radiative) excitons is replaced by $2\pi/L^*$.

Thus, the radiative lifetime $\tau(T)$ ($T \gg \Delta^*/k_B$) is now given by

$$\tau(T) \simeq \begin{cases} \tau_0^*\sqrt{\pi k_B T/4\Delta^*} & \text{(1D)} \\ \tau_0^*(k_B T/\Delta^*) & \text{(2D)} \end{cases} \tag{3}$$

where

$$\tau_0^{*-1} = \begin{cases} 6\pi^3(L^*/a)\gamma_s & \text{(1D)} \\ 6\pi(L^*/a)^2\gamma_s & \text{(2D).} \end{cases}$$

We note here, however, that the final expression for $\tau(T)$ is unchanged from equations (1) and (3) as long as $T \gg \Delta^*/k_B$ holds. Although τ_0 is replaced by τ_0^* and Δ by Δ^* in the presence of large homogeneous broadening, the L^*-dependence disappears in equation (3), since $\Delta^* \sim h^2/2ML^{*2}$.

This fact justifies the determination of the intrinsic radiative lifetime τ_0 from the observed lifetime $\tau(T)$ using the original Δ and equation (1). We can now compare the expressions of equation (1) with the data in figure 23. The observed lifetime below 60 K, where radiative decay is dominant, is indeed fitted by $92\sqrt{T}$ ps $K^{-1/2}$ for the QWRs and $24T$ ps K^{-1} for the top-QWs, as shown by the curves in figure 23. By comparing these results with equation (1), we find that the intrinsic radiative lifetime τ_0 of the $K \sim 0$ exciton is 110 ps in the QWRs and 26 ps in the top-QWs; τ_0 is longer in 1D than in 2D.

Equation (2) clearly explains why the observed τ_0 is longer in 1D than in 2D: τ_0^{-1} for 1D is enhanced by a factor of λ/a, whereas τ_0^{-1} for 2D is enhanced by $(\lambda/a)^2$. Although itis

thought that the parameter a for 1D excitons can become small, this effect is not sufficient to overcome the difference of the 1D and 2D enhancement factors.

9. Laser action

The desire to realize QWR lasers with low thresholds, reduced temperature sensitivities, and increased modulation bandwidths has been one of the most important motivations of QWR study (reference [115]). The study of QWR lasers carried out before 1991 has been reviewed in the paper by Kapon [36, 37].

In 1989, Kapon and co-workers [33] reported the first observation of lasing, or stimulated emission, in a V-groove QWR laser diode structure. The QWR lasers are grown on a V-grooved substrate, as otherwise conventional GaAs/$Al_xGa_{1-x}As$ separate-confinement single-QW laser structures formed in p–n junctions. Due to the sharp bending of the optical waveguide layer, a 1D optical waveguide for light is formed on each V groove, which surrounds the QWRs for electrons and holes. This 1D optical waveguide is important for enhancing the optical confinement factor in the extremely narrow wires. The lasing measurement was made at room temperature and by current injection. Since the QWRs are of rather large size (80–100 nm $\times$ 10 nm), the subband separation was about 10 meV, and many subbands were occupied in the first report. However, the stimulated emission was observed not from the QWR ground states but only from the higher-order QWR subbands with higher gain.

Then, Kapon and co-workers improved the structures [34, 37] by making smaller QWRs, multiple stacks of QWRs, denser arrays of QWRs, and by optimizing the optical waveguides. As a result, a low threshold current of 0.6 mA was achieved at room temperature [35]. Still, however, the stimulated emission was observed only from the higher-order QWR subbands with higher gain.

In 1993, Wegscheider and co-workers [9, 11] demonstrated stimulated emission from the ground-state excitons for the first time in 7 nm-scale GaAs/$Al_{0.35}Ga_{0.65}As$ T-QWRs. The 22 periods of T-QWRs were formed in combination with a T-shaped 1D optical waveguide to realize 1D separate confinement. They cleaved the wafer into a laser bar bounded by two mirrors of uncoated cleaved surfaces with the optical cavity length of 600 μm. At low temperature and by optical pumping, they studied the emission properties of this structure. When the excitation level was low, spontaneous emission from excitons in QWRs was observed, which showed closely ($\sim$0.2 meV) spaced Fabry–Pérot oscillations corresponding to different longitudinal modes within the cavity. When it was increased up to 10 mW, or 600 kW cm^{-2}, the excitonic PL was changed into multimode stimulated emission. When it was increased up to 50 mW, or 3 kW cm^{-2}, the stimulated emission converged into single-mode emission, with the central emission energy unchanged.

It was thus concluded that the observed QWR response was due to exciton recombination, because the emission energy was nearly independent of the pumping level over three orders of magnitude from low-power PL to a single-mode lasing. The absence of band-gap renormalization demonstrated the stability of the 1D excitons in QWRs. Wegscheider and co-workers pointed out that the observed $E^*_{1D-2D} = 17$ meV also suggested an enhancement of the 1D exciton binding energy by more than 50%.

In 1994, Wegscheider and co-workers succeeded in achieving QWR laser operation with current injection [10], which was also studied under strong magnetic fields up to 12 T [12].

It should also be mentioned that not only these cleaved-edge-cavity structures, but also vertical-cavity surface-emitting laser structures have been studied in combination with QWRs [49, 70].

10. Other properties

In spite of the recent increase in interest in ever more advanced properties of 1D excitons in QWRs such as many-body effects, and processes of relaxation via phonon scattering or carrier–carrier scattering, these problems are still not resolved.

The first subject to discuss in this section is band-gap renormalization (BGR), or many-body effects expected for excitons in QWRs at high excitation density. In 2D and 3D systems at high carrier density, the screening of the Coulomb interaction by many carriers makes excitons quench and decompose into free-electron–hole plasma, which shows BGR, or reduced band gaps.

For QWRs, several papers have been rather controversial. We quote the summing up of the situation from one of the recent papers [43]. 'Experimental reports range from evidence for a very large band-gap energy shift [87, 90], to no shift at all [9, 40, 41], with some authors observing shifts only due to the carriers in other subbands [91]'.

As far as QWRs in the strong-confinement regime are concerned, however, experiment appears to show no BGR but stable excitons even at high excitation densities of more than 10^6 cm^{-1}. The PL and CL measurements for small T-QWRs and V-groove QWRs for various excitation densities have typically shown some broadening but almost no shifts from the excitonic peak observed at the lowest excitation density [9, 40, 41, 43].

The next subject is Fermi-edge singularity (FES), or many-body effects expected for excitons in doped QWRs with excess electrons. It is known for doped 2D and 3D systems that optical transitions occur basically between free electrons and holes, in which the Coulomb correlation effect appears as the FES, or an enhanced transition at the Fermi edge, instead of an excitonic transition below the energy gap. There have been a few experimental reports of FESs in QWRs [68, 92–94], though only in weakly confined or large QWRs.

Calleja and co-workers [93, 94] studied 100 nm-wide and 200 nm-period GaAs QWRs processed from a modulation-doped single QW with 25 nm thickness by electron-beam lithography and low-energy-ion bombardment which deplete the QWs in lines. Since the 1D energy modulation is formed by the electrostatic potential, the electrons and holes are confined in spatially separated wires (type II QWRs). They reported strong differences in the PL and PLE spectra between the QWRs and the reference QW—that is, the increased strength of the FES in QWRs over that for QWs. They found a strong temperature dependence and an effect of interference between the FES and the excitonic resonance of unoccupied 1D subbands.

Fritze and co-workers [92] studied 50 nm-wide and 200 nm-period $In_xGa_{1-x}As$ and GaAs QWRs (type II QWRs) processed from n-type asymmetrically doped single QWs of 15 nm thickness by holographic lithography and selective wet etching. They reported the strong FES in $In_xGa_{1-x}As$ QWRs as a spatially direct transition. It was strongly temperature dependent, showing broadening, and diminishing in intensity by the time the temperature reached 30 K.

Mélin and Laruelle [68] studied the FES in n-doped lateral SL QWRs formed on vicinal substrates. Although the confinement was weak for electrons, the electrons and holes were confined in identical wires (type I QWRs). By varying the tilting angle in the lateral SL, they tuned the potential modulation to change the electron–hole overlap and the hole dimensionality between 1D and 2D [66, 67]. The coupling effect of different QW subbands on the FES, and the enhancement of the FES for the strong electron–hole overlap were observed, in agreement with theories.

The third subject to be mentioned here is the reduction or modification of the relaxation

processes of 1D excitons in QWRs. This has been one of the most important motivations of QWR study aimed at realizing reduced relaxation, with a view to achieving high electron mobility and small optical transition linewidths. Such reduction of the relaxation by phonon scattering or carrier–carrier scattering was predicted theoretically to occur in low-dimensional structures as a result of energy and momentum conservation (reference [116]). A similar effect has been intensively investigated for quantum dots as the phonon-bottleneck effect (reference [117]).

There have been several experiments claiming the observation of such an effect [51, 81, 84, 88]. On the other hand, the absence of such expected effects within experiments on so-far-studied QWR samples has also been discussed in unpublished or published forms [39]. In particular, for QWRs with strong-confinement regimes, strong evidence of such an effect has not yet been reported to the best of the author's knowledge.

The critical problem in practice is that small QWRs with tight confinement tend to have large broadening in the PL—that is, increased roughness scattering and/or inhomogeneity. We should note the general requirement that QWRs must be uniform and have a small degree of broadening so as not to disturb the phenomena of interest. Further improvement in sample quality is crucial to the investigation of subtle or advanced physics.

The final subject in this section is the importance of local optical spectroscopy, such as micro-PL [24], CL with scanning electron-beam excitation [38], and near-field scanning optical microscopy [11, 30], in QWR study.

These methods were introduced firstly to assign PL and CL signals to the constituent QWRs and other structures. In addition, instead of studying the averaged properties of many QWRs, we should investigate the various regions of individual QWRs. The photo-excited carrier flow and diffusion also merits study. As discussed above, advanced study of QWR physics is currently limited by the quality of the QWR samples. Thus, the detailed characterization of spatially dependent sample quality is very important, not only to the study of the samples themselves but also for improving the fabrication technique.

It should be commented that such local spectroscopy across the QWR directions has been successful in ascribing signals to QWRs, whereas that along the QWR direction has very often proven the localized or inhomogeneous nature of QWRs like 'quantum sausages'.

Therefore, it is useful to measure PL spectra for the QWR region by scanning the excitation position along the wire direction and demonstrating the uniformity of the electronic states of the QWRs. Figure 25 shows such PL spectra measured by Yoshita and SSA at 5 K for the 3.5 nm-scale $In_{0.17}Ga_{0.83}As$ T-QWR sample shown in figure 11. Although figure 11 shows PL spectra for only one point, figure 25 shows measurements for the QWR region along the wire direction in steps of 1 μm to a total 50 μm length. These spectra demonstrate that the PL signal of each peak is nearly constant along the wire direction and that the peak position does not move. This feature was reproduced over the whole sample range of about 2 mm. The uniformity of the PL spectra of the QWR along the wire direction confirms that high-quality and uniform $In_{0.17}Ga_{0.83}As$ T-QWRs were formed.

Yoshita and SSA also presented a spectrally integrated PL intensity image measured at 5 K from the top (110) surface of the same 3.5 nm-scale $In_{0.17}Ga_{0.83}As$ T-QWR sample [24]. The spatial resolution was 1 μm for the PL wavelength of $\lambda = 780$ nm through the 1.5 mm glass window of the cryostat. The excitation was produced uniformly by a He–Ne laser. Bright PL was observed very uniformly along the wires. Such uniform images were obtained over the whole region of the sample. This result means that uniform $In_{0.17}Ga_{0.83}As$ QWRs and QWs were formed by a successful CEO process. It is useful to perform these measurements on various, sometimes unsuccessfully fabricated, samples, because they sensitively show the consequences of slight deviation from the optimized

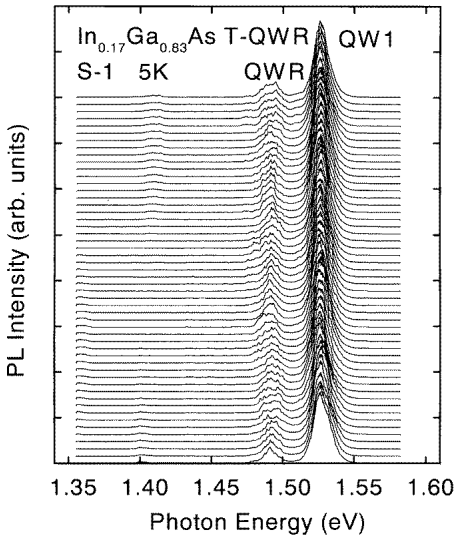

Figure 25. PL spectra of a 3.5 nm-scale T-QWR sample of $In_{0.17}Ga_{0.83}As/Al_{0.3}Ga_{0.7}As$ at 5 K with point photo-excitation of the QWR region. The probed position was scanned along the wire direction in steps of 1 μm. The PL spectra were obtained for a total length of 50 μm along the wire direction. (Reproduced from reference [24].)

growth and/or processing conditions for fabricating QWRs. Using focused-spot excitation instead of uniform excitation reveals carrier flow and diffusion processes in QWR structures.

11. Summary and notes

The elementary properties of 1D excitons in GaAs QWRs, which demonstrate some novel physics inherent to 1D systems, have been reviewed. On the other hand, the studies of these properties are still strongly limited by the quality of the QWR samples, and thus these are mostly performed at low temperatures and as very sophisticated experiments. The direct observation of 1D DOSs, room temperature QWR ground-state lasers, and many other fundamental experiments have not yet been accomplished. We finally emphasize the well-recognized importance of continuous efforts to improve the fabrication and the characterization of QWRs to make progress in 1D physics.

Acknowledgments

The author acknowledges his collaborators, especially Professor H Sakaki, Drs T Someya, S Koshiba, and M Yoshita, for their contribution to the work performed at the University of Tokyo described in this review. He also thanks Drs T D Harris, L N Pfeiffer, J Hasen, K W West, and A Pinczuk, for their hospitality and fruitful discussions during his stay at Bell Laboratories for four months (February–May 1996). This work was supported by the PRESTO programme (October 1993–September 1996) of the Japan Science and Technology Corporation (JST), and is currently supported by a Grant-in-Aid from the Ministry of Education, Science, Sports, and Culture of Japan.

References

[1] Weisbuch C and Vinter B 1991 *Quantum Semiconductor Structures: Fundamentals and Applications* (San Diego, CA: Academic)
[2] Sakaki H and Noge H 1994 *Nanostructures and Quantum Effects* (Berlin: Springer)

[3] Bastard G 1988 *Wave Mechanics Applied to Semiconductor Heterostructures* (New York: Halsted)
[4] Chang Y C, Chang L L and Esaki L 1985 *Appl. Phys. Lett.* **47** 1324
[5] Pfeiffer L N, West K W, Störmer H L, Eisenstein J P, Baldwin K W, Gershoni D and Spector J 1990 *Appl. Phys. Lett.* **56** 1697
[6] Pfeiffer L N, Störmer H L, Baldwin K W, West K W, Goñi A R, Pinczuk A, Ashoori R C, Dignam M M and Wegscheider W 1993 *J. Cryst. Growth* **127** 849
[7] Someya T, Akiyama H and Sakaki H 1996 *J. Appl. Phys.* **79** 2522
[8] Goñi A R, Pfeiffer L N, West K W, Pinczuk A, Baranger H U and Störmer H L 1992 *Appl. Phys. Lett.* **61** 1956
[9] Wegscheider W, Pfeiffer L N, Dignam M M, Pinczuk A, West K W, McCall S L and Hull R 1993 *Phys. Rev. Lett.* **71** 4071
[10] Wegscheider W, Pfeiffer L N, West K W and Leibenguth R E 1994 *Appl. Phys. Lett.* **65** 2510
[11] Grober R D, Harris T D, Trautman J K, Betzig E, Wegscheider W, Pfeiffer L N and West K W 1994 *Appl. Phys. Lett.* **64** 1421
[12] Wegscheider W, Pfeiffer L N, West K, Littlewood P, Narayan O, Hagn M, Dignam M M and Leibenguth R E 1996 *Solid-State Electron.* **40** 1
[13] Pfeiffer L N, Baranger H, Gershoni D, Smith K and Wegscheider W 1995 *Low Dimensional Structures Prepared by Epitaxial Growth or Regrowth on Patterned Substrates (NATO Advanced Study Institute, Series E: Applied Sciences, vol 298)* ed K Ebel *et al* (Dordrecht: Kluwer) p 93
[14] Someya T, Akiyama H and Sakaki H 1995 *Appl. Phys. Lett.* **66** 3672
The structure parameters indicated in the original paper were later re-calibrated to the values shown in this review.
[15] Someya T, Akiyama H and Sakaki H 1995 *Phys. Rev. Lett.* **74** 3664
The structure parameters indicated in the original paper were later re-calibrated to the values shown in this review.
[16] Someya T, Akiyama H and Sakaki H 1996 *Phys. Rev. Lett.* **76** 2965
[17] Someya T, Akiyama H, Yamauchi M, Sugawara H and Sakaki H 1996 *Solid-State Electron.* **40** 315
[18] Someya T, Akiyama H and Sakaki H 1998 unpublished
The data shown in this review are preliminary, and will be published after refinement.
[19] Akiyama H, Someya T and Sakaki H 1996 *Phys. Rev.* B **53** R4229
[20] Akiyama H, Someya T and Sakaki H 1996 *Phys. Rev.* B **53** R10 520
[21] Akiyama H, Someya T and Sakaki H 1996 *Phys. Rev.* B **53** R16 160
[22] Akiyama H, Someya T and Sakaki H 1997 *Mater. Sci. Eng.* B **48** 126
[23] Akiyama H, Someya T, Yoshita M, Sasaki T and Sakaki H 1998 *Phys. Rev.* B **57** 3765
[24] Yoshita M, Akiyama H, Someya T and Sakaki H 1998 *J. Appl. Phys.* **83** 3777
[25] Hasen J, Pfeiffer L N, Pinczuk A, Baranger H U, West K W and Dennis B S 1997 *Superlatt. Microstruct.* **22** 359
[26] Gislason H, Langbein W and Hvam J M 1996 *Appl. Phys. Lett.* **69** 3248
[27] Langbein W, Gislason H and Hvam J M 1996 *Phys. Rev.* B **54** 14 595
[28] Gershoni D, Weiner J S, Chu S N G, Baraff G A, Vandenberg J M, Pfeiffer L N, West K, Logan R A and Tanbun-Ek T 1990 *Phys. Rev. Lett.* **65** 1631
Gershoni D, Weiner J S, Chu S N G, Baraff G A, Vandenberg J M, Pfeiffer L N, West K, Logan R A and Tanbun-Ek T 1991 *Phys. Rev. Lett.* **66** 1375
Kash K, Mahoney D D and Cox H M 1991 *Phys. Rev. Lett.* **66** 1374
[29] Gershoni D, Katz M, Wegscheider W, Pfeiffer L N, Logan R A and West K 1994 *Phys. Rev.* B **50** 8930
[30] Harris T D, Gershoni D, Grober R D, Pfeiffer L N, West K W and Chaud N 1996 *Appl. Phys. Lett.* **68** 988
[31] Kapon E, Tamargo M C and Hwang D M 1987 *Appl. Phys. Lett.* **50** 347
[32] Bhat R, Kapon E, Hwang D M, Koza M A and Yun C P 1988 *J. Cryst. Growth* **93** 850
[33] Kapon E, Hwang D M and Bhat R 1989 *Phys. Rev. Lett.* **63** 430
[34] Kapon E, Kash K, Clausen E M Jr, Hwang D M and Colas E 1992 *Appl. Phys. Lett.* **60** 477
[35] Simhony S, Kapon E, Colas E, Hwang D M, Stoffel N G and Worland P 1991 *Appl. Phys. Lett.* **59** 2225
[36] Kapon E 1992 *Proc. IEEE* **80** 398
[37] Kapon E, Walther M, Christen J, Grundmann M, Caneau C, Hwang D M, Colas E, Bhat R, Song G H and Bimberg D 1992 *Superlatt. Microstruct.* **12** 491
[38] Christen J, Kapon E, Grundmann M, Hwang D M, Joschko M and Bimberg D 1992 *Phys. Status Solidi* b **173** 307
[39] Christen J, Grundmann M, Kapon E, Colas E, Hwang D M and Bimberg D 1992 *Appl. Phys. Lett.* **61** 67
[40] Grundmann M, Christen J, Joschko M, Stier O, Bimberg D and Kapon E 1994 *Semicond. Sci. Technol.* **9**

1939
[41] Gustafsson A, Reinhardt F, Biasiol G and Kapon E 1995 *Appl. Phys. Lett.* **67** 3673
[42] Vouilloz F, Oberli D Y, Dupertuis M-A, Gustafsson A, Reinhardt F and Kapon E 1997 *Phys. Rev. Lett.* **78** 1580
[43] Ambigapathy R, Bar-Joseph I, Oberli D Y, Haacke S, Brasil M J, Reinhardt F, Kapon E and Deveaud B 1997 *Phys. Rev. Lett.* **78** 3579
[44] Rinaldi R, Cingolani R, Lepore M, Ferrara M, Catalano I M, Rossi F, Rota L, Molinari E, Lugli P, Marti U, Martin D, Morier-Gemoud F, Ruterana P and Reihart F K 1994 *Phys. Rev. Lett.* **73** 2899
[45] Rinaldi R, Ferrara M, Cingolani R, Marti U, Martin D, Morier-Gemoud F, Ruterana P and Reihart F K 1994 *Phys. Rev.* B **50** 11 795
[46] Nagamune Y, Arakawa Y, Tsukamoto S, Nishioka M, Sasaki S and Miura N 1992 *Phys. Rev. Lett.* **69** 2963
[47] Tsukamoto S, Nagamune Y, Nishioka M and Arakawa Y 1993 *Appl. Phys. Lett.* **63** 355
[48] Kono T, Tsukamoto S, Nagamune Y, Sogawa F, Nishioka M and Arakawa Y 1994 *Appl. Phys. Lett.* **64** 1564
[49] Arakawa T, Nishioka M, Nagamune Y and Arakawa Y 1994 *Appl. Phys. Lett.* **64** 2200
[50] Nagamune Y, Tanaka T, Kono T, Tsukamoto S, Nishioka M, Arakawa Y, Uchida K and Miura N 1995 *Appl. Phys. Lett.* **66** 2502
[51] Nagamune Y, Watabe H, Sogawa F and Arakawa Y 1995 *Appl. Phys. Lett.* **67** 1535
[52] Sogawa T, Ando H, Ando S and Kanbe H 1997 *Phys. Rev.* B **56** 1958
[53] Koshiba S, Noge H, Akiyama H, Inoshita T, Nakamura Y, Shimizu A, Nagamune Y, Tsuchiya M, Kano H, Sakaki H and Wada K 1994 *Appl. Phys. Lett.* **64** 363
[54] Koshiba S, Noge H, Ichinose H, Akiyama H, Nakamura Y, Inoshita T, Someya T, Wada K, Shimizu A and Sakaki H 1994 *Solid-State Electron.* **37** 729
[55] Akiyama H, Koshiba S, Someya T, Wada K, Noge H, Nakamura Y, Inoshita T, Shimizu A and Sakaki H 1994 *Phys. Rev. Lett.* **72** 924
Akiyama H, Koshiba S, Someya T, Wada K, Noge H, Nakamura Y, Inoshita T, Shimizu A and Sakaki H 1994 *Phys. Rev. Lett.* **72** 2123
[56] Akiyama H and Sakaki H 1995 *Mater. Sci. Eng.* B **35** 284
[57] Petroff P M, Gossard A C and Wiegmann W 1984 *Appl. Phys. Lett.* **45** 620
[58] Gaines J M, Petroff P M, Kroemer H, Simes R J, Geels R S and English J H 1988 *J. Vac. Sci. Technol.* B **6** 1378
[59] Krishnamurthy M, Lorke A, Wassermeier M, Williams D R M and Petroff P M 1993 *J. Vac. Sci. Technol.* B **11** 1384
[60] Fukui T and Saito H 1987 *Appl. Phys. Lett.* **50** 824
[61] Tsuchiya M, Gaines J M, Yan R H, Simes R J, Holtz P O, Coldren L A and Petroff P M 1989 *Phys. Rev. Lett.* **62** 466
Weman H, Miller M S and Merz J L 1992 *Phys. Rev. Lett.* **68** 3656
[62] Tanaka M and Sakaki H 1989 *Appl. Phys. Lett.* **54** 1326
[63] Miller M S, Weman H, Pryor C E, Krishnamurthy M, Petroff P M, Kroemer H and Merz J L 1992 *Phys. Rev. Lett.* **68** 3464
[64] Weman H, Miller M S, Pryor C E, Li Y J, Bergman P, Petroff P M and Merz J L 1993 *Phys. Rev.* B **48** 8047
[65] Weman H, Jones E D, McIntyre C R, Miller M S, Petroff P M and Merz J L 1993 *Superlatt. Microstruct.* **13** 5
[66] Bloch J, Bockelmann U and Laruelle F 1994 *Europhys. Lett.* **28** 501
[67] Bloch J, Bockelmann U and Laruelle F 1994 *Solid-State Electron.* **37** 529
[68] Mélin T and Laruelle F 1996 *Phys. Rev. Lett.* **76** 4219
[69] Kanbe H, Chavez-Pirson A, Ando H, Saito H and Fukui T 1991 *Appl. Phys. Lett.* **58** 2969
[70] Chavez-Pirson A, Ando H, Saito H and Kanbe H 1994 *Appl. Phys. Lett.* **64** 1759
[71] Nötzel R, Ledentsov N N, Daweritz L, Hohenstein M and Ploog K 1991 *Phys. Rev. Lett.* **67** 3812
[72] Nötzel R, Ramsteiner M, Menniger J, Trampert A, Schonherr H-P, Daweritz L and Ploog K H 1996 *J. Appl. Phys.* **80** 4108
[73] Hara S, Motohisa J, Fukui T and Hasegawa H 1995 *Japan. J. Appl. Phys.* **34** 4401
[74] Mayer G, Maile B E, Germann R, Forchel A, Grambow P and Meier H P 1990 *Appl. Phys. Lett.* **56** 2016
[75] Kohl M, Heitmann D, Ruhle W W, Grambow P and Ploog K 1990 *Phys. Rev.* B **41** 12 338
[76] Notomi M, Naganuma M, Nishida T, Tamamura T, Iwamura H, Nojima S and Okamoto M 1991 *Appl. Phys. Lett.* **58** 720
[77] Marzin J Y, Izrael A and Birotheau L 1994 *Solid-State Electron.* **37** 1091

[78] Kash K, Worlock J M, Sturge M D, Grabbe P, Harbison J P, Scherer A and Lin P S D 1988 *Appl. Phys. Lett.* **53** 782
[79] Gréus Ch, Butov L, Daiminger F, Forchel A, Knipp P A and Reinecke T L 1993 *Phys. Rev.* B **47** 7626
[80] Kash K, Bhat R, Mahoney D D, Lin P S D, Scherer A, Worlock J M, Van der Gaag B P, Koza M and Grabbe P 1989 *Appl. Phys. Lett.* **55** 681
[81] Mayer G, Prins F E, Lehr G, Schweizer H, Leier H, Maile B E, Straka J, Forchel A and Weimann G 1993 *Phys. Rev.* B **47** 4060
[82] Kohl M, Heitmann D, Grambow P and Ploog K 1989 *Phys. Rev. Lett.* **63** 2124
[83] Plaut A S, Lage H, Grambow P, Heitmann D, von Klitzing K and Ploog K 1991 *Phys. Rev. Lett.* **67** 1642
[84] Cingolani R, Lage H, Tapfer L, Kalt H, Heitmann D and Ploog K 1991 *Phys. Rev. Lett.* **67** 891
[85] Cingolani R, Lepore M, Tommasi R, Catalano I M, Lage H, Heitmann D, Ploog K, Shimizu A, Sakaki H and Ogawa T 1992 *Phys. Rev. Lett.* **69** 1276
[86] Cingolani R, Lepore M, Tommasi R, Catalano I M, Lage H, Heitmann D, Ploog K, Shimizu A, Sakaki H and Ogawa T 1993 *Superlatt. Microstruct.* **13** 71
[87] Cingolani R, Rinaldi R, Ferrara M, Lage H, Heitmann D, Ploog K and Kalt H 1993 *Phys. Rev.* B **48** 14 331
[88] Oestreich M, Ruhle W W, Lage H, Heitmann D and Ploog K 1993 *Phys. Rev. Lett.* **70** 1682
[89] Mayer E J, White J O, Smith G O, Lage H, Heitmann D, Ploog K and Kuhl J 1994 *Phys. Rev.* B **49** 2993
[90] Gréus Ch, Forchel A, Spiegel R, Faller F, Benner S and Haug H 1996 *Europhys. Lett.* **34** 213
[91] Wang K H, Bayer M, Forchel A, Ils P, Benner S, Haug H, Pagnod-Rossiaux P and Goldstein L 1996 *Phys. Rev.* B **53** R10 505
[92] Fritze M, Nurmikko A V and Hawrylak P 1993 *Phys. Rev.* B **48** 4960
[93] Calleja J M, Goñi A R, Dennis B S, Weiner J S, Pinczuk A, Schmitt-Rink S, Pfeiffer L N, West K W, Muller J F and Ruckenstein A E 1991 *Solid State Commun.* **79** 911
[94] Calleja J M, Goñi A R, Pinczuk A, Dennis B S, Weiner J S, Pfeiffer L N and West K W 1995 *Phys. Rev.* B **51** 4285
[95] Someya T, Akiyama H and Sakaki H 1996 *Japan. J. Appl. Phys.* **35** 2544
[96] Tarucha S, Okamoto H, Iwasa Y and Miura N 1984 *Solid State Commun.* **52** 815
[97] Miller D A B, Chemla D S, Eilenberger D J, Smith P W, Gossard A C and Tang W T 1982 *Appl. Phys. Lett.* **41** 679
[98] Loudon R 1959 *Am. J. Phys.* **27** 649
Elliott R J and Loudon R 1960 *J. Phys. Chem. Solids* **15** 196
[99] Ogawa T and Takagahara T 1991 *Phys. Rev.* B **43** 14 325
Ogawa T and Takagahara T 1991 *Phys. Rev.* B **44** 8138
[100] Sercal P C and Vahala K J 1990 *Appl. Phys. Lett.* **57** 545
[101] Citrin D S and Chang Y-C 1991 *Phys. Rev.* B **43** 11 703
[102] Ando H, Nojima S and Kanbe H 1993 *J. Appl. Phys.* **74** 6383
[103] Bauer G E W and Sakaki H 1992 *Surf. Sci.* **267** 442
[104] Weiner J S, Chemla D S, Miller D A B, Haus H A, Gossard A C, Wiegmann W and Burrus C A 1985 *Appl. Phys. Lett.* **47** 664
[105] Gershoni D, Brener I, Baraff G A, Chu S N G, Pfeiffer L N and West K 1991 *Phys. Rev.* B **44** 1930
[106] Yamaguchi A A and Usui A 1995 *J. Appl. Phys.* **78** 1361
Yamaguchi A A, Nishi K and Usui A 1994 *Japan. J. Appl. Phys.* **33** L912
[107] McIntyre C R and Sham L J 1992 *Phys. Rev.* B **45** 9443
[108] Akimoto O and Hasegawa H 1967 *J. Phys. Soc. Japan* **22** 181
[109] Sakaki H, Arakawa Y, Nishioka M, Yoshino J, Okamoto H and Miura N 1985 *Appl. Phys. Lett.* **46** 83
[110] Masumoto Y, Matsuura M, Tarucha S and Okamoto H 1985 *Phys. Rev.* B **32** 4275
[111] Feldmann J, Peter G, Göbel E O, Dawson P, Moore K, Foxon C and Elliott R J 1987 *Phys. Rev. Lett.* **59** 2337
[112] Andreani L C 1991 *Solid State Commun.* **77** 641
[113] Citrin D S 1992 *Phys. Rev. Lett.* **69** 3393
[114] Hanamura E 1988 *Phys. Rev.* B **15 38** 1228
[115] Arakawa Y and Sakaki H 1982 *Appl. Phys. Lett.* **40** 939
[116] Sakaki H 1980 *Japan. J. Appl. Phys.* **19** L735
[117] Benisty H, Sotomayor-Torres C M and Weisbuch C 1991 *Phys. Rev.* B **44** 10 945